Mon. Not. R. Astron. Soc. **342,** 86–104 (2003)

Obscured asymptotic giant branch variables in the Large Magellanic Cloud and the period–luminosity relation

Patricia A. Whitelock,[1⋆] Michael W. Feast,[2] Jacco Th. van Loon[3] and Albert A. Zijlstra[4]

[1]*South African Astronomical Observatory, PO Box 9, 7935 Observatory, South Africa*
[2]*Astronomy Department, University of Cape Town, 7701 Rondebosch, South Africa*
[3]*Astrophysics Group, School of Chemistry & Physics, Keele University, Staffordshire ST5 5BG*
[4]*Department of Physics, UMIST, PO Box 88, Manchester M60 1QD*

Accepted 2003 February 10. Received 2003 February 10; in original form 2003 January 3

ABSTRACT

The characteristics of oxygen-rich and carbon-rich, large-amplitude ($\Delta K > 0.4$ mag), asymptotic giant branch (AGB) variables in the Large Magellanic Clouds are discussed, with an emphasis on those obscured by dust. Near-infrared photometry, obtained over about 8 yr, is combined with published mid-infrared observations from *IRAS* and *ISO* to determine bolometric magnitudes for 42 stars. Pulsation periods of the O-rich stars are in the range $116 < P < 1393$ d, while those for C-rich stars have $298 < P < 939$ d. In addition to the regular pulsations, one O-rich star and four C-rich stars show large-amplitude, $\Delta K > 0.6$ mag, secular or very long-period variations, which may be associated with changes in their mass-loss rates. We discuss and compare various methods of determining the bolometric magnitudes and show, perhaps surprisingly, that most of the very long-period stars seem to follow an extrapolation of the period–luminosity relation determined for stars with shorter periods – although the details do depend on how the bolometric magnitudes are calculated.

Three stars with thin shells, which are clearly more luminous than the obscured AGB stars, are undergoing hot bottom burning, while other stars with similar luminosities have yet to be investigated in sufficient detail to determine their status in this regard. We suggest that an apparent change in slope of the period–luminosity relation around 400–420 d is caused by variables with luminosities brighter than the predictions of the core-mass–luminosity relation, owing to excess flux from hot bottom burning.

Key words: stars: AGB and post-AGB – stars: carbon – stars: mass-loss – stars: variables: other – Magellanic Clouds – infrared: stars.

1 INTRODUCTION

Stars at the top of the asymptotic giant branch (AGB) are of interest, primarily for two reasons. First, they are undergoing mass loss – via mechanisms that are still poorly understood. Secondly, they represent the most luminous phase in the evolution of low- and intermediate-mass stars and, as high-resolution techniques enable us to examine stars in ever more distant galaxies, are therefore among the first individual objects to be isolated in a given population; furthermore, they will contribute a significant fraction of the IR (infrared) luminosity of distant unresolved populations (Ferraro et al. 1995; Mouhcine & Lançon 2002). The Large Magellanic Cloud (LMC) provides a particularly useful laboratory for the studies of luminous AGB stars at a known distance but with a range of initial masses.

Two factors complicate the studies of these luminous AGB stars: their long-period large-amplitude variability, which necessitates observations over periods of many years, and their high mass-loss rates, which lead to thick dust shells and necessitate observations at mid-infrared wavelengths. Earlier papers in this series (Loup et al. 1997, hereafter Paper I; Zijlstra et al. 1996, hereafter Paper II; van Loon et al. 1997, 1998, hereafter Papers III and IV; Trams et al. 1999b, hereafter Paper V; van Loon et al. 1999, hereafter Paper VI) described the identification of luminous AGB stars in the LMC, using *IRAS* and *JHKL* photometry, as well as extensive *ISO* observations of a subset of them, and the derivation of their mass-loss rates.

This paper concentrates on the variability characteristics of the sample, reporting near-infrared (*JHKL*) photometry obtained in

⋆E-mail: paw@saao.ac.za

support of the spectroscopy and mid-infrared photometry discussed in previous papers (see Papers I–VI). These data, together with others from the literature, are used to determine pulsation periods and amplitudes and to look for long-term trends in the behaviour of the stars. They are also combined with the observations discussed previously to determine the bolometric magnitudes and examine their relationship with the pulsation characteristics of the stars.

It is known that stars near to the end of their AGB evolution are large-amplitude, reasonably regular pulsators and that stars with these characteristics form a well-defined group (e.g. Whitelock 2003 and references therein). As the intention here is to consider stars very near to the tip of the AGB, we use the information at our disposal to isolate the objects of interest, removing from the sample supergiants as well as semiregular and irregular pulsators.

Following Feast, Whitelock & Menzies (2002) we assume here that the distance modulus of the LMC is $(m - M)_0 = 18.60$ mag, and, where necessary, the results of other analyses are corrected to this value.

1.1 Hot bottom burning (HBB)

Towards the end of AGB evolution, in stars with initial masses in excess of 4 or 5 $M_\odot$ (or perhaps at even lower masses for very low metallicities), the base of the H-rich convective envelope can dip into the H-burning shell; the introduction of fresh H-rich material into the nuclear-burning shell allows the luminosity to go above the core-mass–luminosity predictions (Blöcker & Schönberner 1991). This process is known as envelope burning or hot bottom burning. Carbon is burned to nitrogen, affecting the transition from oxygen-rich to carbon-rich, although the details depend on the model and particularly on how mass loss is treated. HBB may prevent C stars from forming at all until the envelope mass is depleted (Frost et al. 1998), although in some models C stars do form and HBB turns the stars back from C-rich to O-rich. Another consequence, for stars in a rather narrow mass range, is the formation of lithium and its mixing to the surface via the beryllium transport mechanism (Sackmann & Boothroyd 1992). Smith et al. (1995) surveyed luminous AGB stars in the LMC and SMC for lithium, the clearest indication that HBB is taking place.

Two stars in our sample are known to be undergoing HBB from the presence of lithium in their spectra (Smith et al. 1995), namely the O-rich star HV 12070 and C-rich star SHV 05210–6904 (SHV F4488). Trams et al. (1999a) showed that the luminous C star, IRAS 04496–6958, has a silicate shell and suggested that it has only very recently stopped HBB. These three stars are of particular interest and are identified in the various diagrams and the discussion which follows.

There are very few LMC stars for which the spectra have been examined for lithium, so none of the others are actually known for certain *not* to be experiencing HBB. Indeed, we would guess that several other stars considered in this paper are in the same condition.

A preliminary analysis of the results from this paper, with an emphasis on the significance of the HBB stars in the period–luminosity (PL) relation, was discussed by Whitelock & Feast (2000).

2 SOURCE SELECTION AND *JHKL* PHOTOMETRY

The coordinates and alternative names of the sources discussed here were listed in Paper I, while Paper II gives the results of the first batch of *JHKL* photometry. In addition to the sources discussed in previous papers in this series we include a few AGB variables previously observed from the South African Astronomical Observatory (SAAO) for which new observations have been obtained. These stars have only thin dust shells, but provide a useful link with the work of Feast et al. (1989), who established a period–luminosity relation from *JHK* observations of these stars and others like them.

Near-infrared (*JHKL*) photometry was carried out between 1993 and 2001 using the Mk III photometer on the SAAO 1.9-m telescope at Sutherland and transformed on to the SAAO standard system defined by Carter (1990). Earlier observations were obtained for some sources as part of other programmes and some of the data published by Feast et al. (1980), Catchpole & Feast (1981) or Glass et al. (1990). The new results are listed in Table 1, which also gives the Julian date (JD) of the observation. Measurements were made through either 12- or 18-arcsec apertures depending on the seeing and the crowding of the individual source. A few of the older observations were made on the 0.75-m telescope through a 36-arcsec aperture – they are marked with an asterisk in the L column. The magnitudes are accurate to better than ± 0.05 mag, unless they are quoted to one decimal place when they are good to ± 0.1 mag. Many of the sources were too faint to measure at J, H or L, particularly near minimum light. It also remains possible that some of the fainter magnitudes quoted at JH have been slightly contaminated owing to the close proximity of other sources.

The *JHKL* observation quoted in Paper II for IRAS 04498–6842 is actually a measure for IRAS 05003–6712. The observation for IRAS 05289–6617 was of the wrong source; only one observation was obtained for the correct object.

The star RHV 0524173–660913 was not part of the *ISO* programme and was observed towards the end of our programme because it appeared to be a particularly luminous C-star. The C spectral type comes from Reid, Hughes & Glass (1995) and its position in a PL relation is shown in fig. 1 of Groenewegen & Whitelock (1996), where it lies well above the standard relation. However, we identify it here with the star that Westerlund, Olander & Hedin (1981) classified as an M giant and which is known as WOH G311 (or WOH G310). It is considered to be an O-rich star in the following discussion, but another spectrum is required to settle the matter. If it really is an M star that has turned into a C star it is obviously extremely interesting and perhaps similar to IRAS 04496–6958 (Trams et al. 1999a). Phased light-curves are shown in Figs 1 and 2 for O-rich and C-rich variables, respectively.

3 PERIODS, AMPLITUDES AND MEAN MAGNITUDES

Table 2 is divided into three parts, the first two containing the summary data for the O- and C-rich AGB stars, using the chemical types determined in earlier papers of this series or from Reid et al. (1995). All of the sources in the first two parts of the table are clearly large-amplitude variables with measurable periods. The Fourier-mean magnitudes (*JHKL*) are listed, as are the number of K observations (n) used to determine the period (P_K) and the full peak-to-peak amplitude at each wavelength (ΔJ, ΔH, ΔK, ΔL). Periods from the literature ($P_{\rm other}$) are also listed and the appropriate references given in the notes. There are five stars for which the mean light is undergoing secular or very long-period variations, these are indicated with an asterisk in the P_K column and are discussed further in Section 4.

The third part of Table 2 contains all of the sources that are not large-amplitude AGB variables or have insufficient data to determine periodicities. Seven of these are supergiants; they have $K <$ 8.0 mag, low-amplitude variability ($\Delta K < 0.4$ mag) and will have

Table 1. Near-infrared photometry for the LMC stars.

JD –244 0000	*J*	*H*	*K*	*L*
		(mag)		
O-rich stars				
HV 12070 (WOH SG 515)				
4287.4	10.6	9.6	9.13	*
4551.6	10.6	9.7	9.27	*
4889.6	10.58	9.65	9.15	
4932.5	10.99	10.07	9.46	*
5011.5	10.76	9.91	9.37	*
5259.6	10.00	9.04	8.68	*
5331.5	9.89	8.88	8.52	
5648.5	10.51	9.52	9.11	*
6034.5	10.09	9.07	8.67	*
6359.5	10.65	9.81	9.36	*
6426.5	10.76	9.85	9.34	*
6442.4	10.63	9.73	9.29	*
6491.4	10.16	9.26	8.87	*
7160.6	10.00	9.00	8.65	
10035.5	10.73	9.88	9.37	8.76
10121.5	10.73	9.81	9.35	8.79
10201.3	10.26	9.36	9.04	8.48
10324.7	9.93	8.89	8.57	8.16
10447.6	10.28	9.28	8.86	8.55
10473.5	10.48	9.48	9.00	8.62
10917.4	9.91	8.82	8.48	7.96
HV 2446 (WOH G274)				
4890.5	10.09	9.04	8.61	
4927.5	10.31	9.26	8.79	*
5036.4	10.91	10.00	9.44	*
5679.5	10.48	9.51	9.03	*
6034.5	10.08	9.01	8.64	*
6360.4	10.70	9.82	9.36	*
6429.4	10.95	10.07	9.63	*
6491.3	10.44	9.50	9.20	*
6794.4	10.66	9.68	9.18	*
9961.7	10.56	9.65	9.19	8.60
10029.4	10.78	9.82	9.34	8.5
10144.4	10.16	9.11	8.73	8.2
10320.7	10.27	9.25	8.82	8.36
10446.5	10.84	9.85	9.32	
10475.4	10.87	9.88	9.36	
10792.6	10.10	9.04	8.66	8.05
IRAS 04407–7000				
6704.6	10.69	9.25	8.50	
6723.4	10.71	9.32	8.55	7.61
6750.5	10.79	9.39	8.64	7.70
6796.4	10.91	9.46	8.69	
6866.3	11.05	9.60	8.85	
7081.5	11.70	10.21	9.27	
7098.5	11.77	10.29	9.33	8.23
7131.5	11.94	10.42	9.41	8.36
7153.4	11.99	10.52	9.49	
7368.6	11.77	10.22	9.20	8.03
7495.5	11.11	9.59	8.69	7.57
9021.3	10.62	9.07	8.23	7.25
9297.5	11.25	9.74	8.86	7.90
9355.3	11.41	9.92	9.01	8.0
9434.2	11.80	10.22	9.23	8.0
9492.2	12.06	10.39	9.32	8.19
9582.7	12.39	10.58	9.43	8.2
9744.4	11.68	10.07	8.98	7.8
9791.3	11.12	9.64	8.70	7.47
9959.6	10.44	8.99	8.20	7.19
10023.6	10.37	8.92	8.15	7.08

Table 1 – *continued*

JD –244 0000	*J*	*H*	*K*	*L*
		(mag)		
IRAS 04407–7000 continued				
10034.5	10.32	8.86	8.12	7.01
10119.3	10.26	8.81	8.10	7.09
10317.6	10.62	9.16	8.43	7.58
10353.6	10.69	9.27	8.51	7.53
10390.5	10.79	9.40	8.61	7.70
10499.4	11.20	9.78	8.93	7.93
IRAS 04498–6842				
9294.5	9.69	8.61	7.92	6.94
9298.5	9.57	8.52	7.89	6.85
9300.5	9.55	8.53	7.87	6.88
9352.3	9.48	8.43	7.80	6.70
9434.3	9.34	8.20	7.64	6.71
9496.2	9.21	8.08	7.52	6.56
9586.6	9.13	7.96	7.43	6.57
9701.4	9.21	8.05	7.52	6.66
9744.4	9.29	8.14	7.64	6.94
9791.3	9.36	8.24	7.69	6.84
9960.6	9.99	8.83	8.20	7.46
10029.4	10.30	9.13	8.42	7.65
10143.3	10.73	9.51	8.67	7.70
10326.5	11.02	9.65	8.71	7.68
10390.5	11.13	9.78	8.77	7.65
10504.3	10.00	8.98	8.18	7.12
10712.6	9.38	8.28	7.67	6.76
10915.2	9.22	8.08	7.50	6.58
11210.4	9.96	8.82	8.18	7.4
11626.2	10.62	9.33	8.52	7.50
IRAS 04509–6922				
9748.4	9.93	8.61	7.95	7.00
9791.3	9.95	8.64	7.97	7.03
9965.6	10.40	9.08	8.38	7.53
10031.4	10.65	9.34	8.59	7.65
10119.3	10.98	9.63	8.80	7.8
10317.6	11.84	10.31	9.30	8.23
10448.5	11.84	10.32	9.29	8.0
10500.4	11.70	10.25	9.22	8.0
10764.4	10.18	8.87	8.14	7.16
10915.3	9.98	8.65	7.95	7.08
IRAS 04516–6902				
7495.6	12.27	10.42	9.28	8.01
9748.4	11.32	9.87	9.00	7.76
9791.4	10.82	9.47	8.66	7.48
10031.4	10.37	8.84	8.11	7.04
10147.2	10.39	8.84	8.12	7.14
10325.6	10.93	9.41	8.66	7.74
10392.5	11.19	9.73	8.92	8.10
10500.4	11.64	10.16	9.24	8.2
10764.4	11.60	10.12	9.23	8.17
10915.3	10.51	9.19	8.43	7.26
11482.6	11.08	9.68	8.87	7.88
IRAS 04545–7000				
9797.3		14.05	11.20	8.6
10031.6		12.09	9.71	7.34
10033.5		12.15	9.73	7.37
10123.4		11.77	9.41	7.11
10320.6		11.80	9.47	7.30
10448.5		12.47	9.79	
10504.3		12.32	9.96	7.74
10761.5		13.06	10.60	8.3
10796.4		13.14	10.70	8.4
10887.3		13.54	10.96	8.6

Table 1 – *continued*

JD –244 0000	*J*	*H*	*K*	*L*
		(mag)		
IRAS 04545–7000 continued				
11095.5		12.82	10.38	8.0
11624.2		11.70	9.56	7.44
11834.6		12.29	10.08	8.08
IRAS 05003–6712				
9022.3	12.62	11.05	9.94	
9742.3	14.2	12.41	10.85	
9959.7	12.36	10.82	9.54	8.00
10027.6	12.11	10.59	9.32	7.82
10123.3	12.06	10.45	9.24	7.86
10325.5	12.77	11.19	9.94	8.46
10392.5	12.96	11.46	10.15	8.85
10474.5	13.4	11.79	10.43	9.0
10764.4	13.26	11.53	10.13	8.6
10796.4	12.82	11.13	9.83	8.3
10915.3	12.23	10.52	9.31	7.86
11095.5	12.14	10.40	9.29	8.0
IRAS 05294–7104				
9964.6	11.38	9.68	8.70	7.4
10032.5	11.46	9.74	8.74	7.57
10327.6	12.57	10.70	9.57	8.44
10501.4	13.36	11.27	9.94	8.4
10705.6	12.20	10.32	9.19	7.92
10889.3	11.47	9.70	8.66	7.38
IRAS 05329–6708				
9024.5			11.65	
9298.4		11.99	9.65	7.38
9747.5		11.61	9.42	7.26
10033.5		12.55	10.27	8.13
10446.5		13.6	10.36	7.9
10501.5		12.17	9.83	7.48
10797.5		11.20	9.07	6.84
10887.4	15.2	11.25	9.14	6.95
IRAS 05402–6956				
10035.6			11.61	8.8
10327.6		12.52	10.10	7.68
10447.5		11.88	9.67	7.45
10504.4		11.71	9.59	7.39
10706.6	14.3	11.33	9.35	7.15
10915.3		11.86	9.79	7.59
11210.5			11.6	
IRAS 05558–7000				
9024.5	11.80	9.93	8.84	7.46
9298.5	12.83	10.88	9.63	8.43
9355.4	13.03	11.07	9.75	8.3
9439.3	13.4	11.29	9.88	8.5
9492.2	13.45	11.30	9.88	8.5
9702.5	12.38	10.47	9.15	7.71
9742.5	12.14	10.18	8.96	7.6
9797.2	11.89	9.96	8.80	7.3
9961.6	11.70	9.73	8.59	7.32
10027.6	11.65	9.71	8.58	7.26
10142.5	11.70	9.84	8.71	7.36
10325.7	12.53	10.68	9.44	8.06
10390.6	12.87	10.99	9.68	8.20
10476.5	13.4	11.35	9.94	
10798.5	13.4	11.47	10.01	8.1
10915.3	12.56	10.75	9.38	7.70
SHV 04544–6848 (SP 30-6)				
9747.3	11.27	10.27	9.55	8.5
9960.6	10.24	9.22	8.76	8.05
10033.5	10.19	9.19	8.67	8.06

Table 1 – *continued*

JD –244 0000	*J*	*H*	*K*	*L*
		(mag)		
SHV 04544–6848 (SP 30-6) continued				
10120.3	10.28	9.24	8.76	8.2
10320.6	11.39	10.29	9.64	8.9
10446.4	10.94	9.96	9.36	
10472.5	10.96	9.97	9.39	
SHV 05220–7012				
9797.4	13.40	12.48	12.05	
10029.5	13.43	12.40	12.02	
10147.3	12.94	11.97	11.53	
10324.7	12.66	11.65	11.39	
10442.5	13.38	12.47	12.08	
10474.5	13.2	12.40	12.01	
10498.4	12.89	11.92	11.64	
SHV 05249–6945				
9963.6	11.61	10.53	10.23	
10029.5	11.71	10.57	10.16	
10144.4	12.58	11.33	10.68	
10323.7	11.92	10.91	10.58	
10442.5	11.69	10.52	10.10	
10504.4	12.18	10.91	10.32	
SHV 05305–7022				
9965.5	12.22	11.32	10.91	
10034.4	11.91	11.02	10.64	
10142.4	11.68	10.66	10.25	
10323.6	12.23	11.34	10.86	
10383.6	12.03	11.15	10.81	
10442.5	11.70	10.66	10.33	
10475.4	11.67	10.61	10.23	
10504.4	11.71	10.67	10.27	
R105				
10387.6	11.92	10.90	10.52	
10498.3	11.45	10.41	10.07	
10602.2	11.74	10.62	10.17	
10762.5	12.00	10.95	10.57	
WBP 74				
10443.4	12.96	11.89	11.46	
10470.5	13.13	12.11	11.65	
10498.3	13.13	12.09	11.76	
10602.3	12.72	11.70	11.26	
10705.6	13.18	12.13	11.71	
10761.6	12.85	12.02	11.53	
GRV 0517584–655140				
10443.4	13.39	12.46	12.2	
10470.4	13.02	12.20	11.91	
10498.3	13.41	12.56	12.20	
10602.2	13.25	12.46	12.14	
10760.6	13.70	12.85	12.5	
RHV 0524173–660913				
8227.5	10.80	9.79	9.37	
10147.2	10.62	9.63	9.24	
10202.3	10.87	9.89	9.47	
10324.7	11.43	10.48	10.00	
10442.4	11.36	10.44	10.05	
10498.3	10.99	10.05	9.71	
10602.3	10.62	9.62	9.28	
10855.4	11.32	10.46	10.01	
10884.3	11.35	10.46	10.02	
10915.3	11.41	10.50	10.08	9.24
C-rich AGB stars				
IRAS 04286–6937				
9020.3		13.58	11.61	9.5
9294.4	12.32	10.48		

Table 1 – *continued*

JD –244 0000	*J*	*H*	*K*	*L*
		(mag)		
IRAS 04286–6937 continued				
9298.4		12.28	10.53	8.4
9742.4		12.93	11.17	
9938.6	14.2	12.02	10.31	8.32
10024.4	14.2	12.11	10.42	8.3
10034.5	14.5	12.13	10.40	8.4
10144.3		12.81	11.01	8.8
10324.6		13.20	11.40	9.3
10387.5		13.20	11.34	9.0
10500.3		12.44	10.63	8.6
11626.2		13.6	11.58	
11890.4		12.42	10.58	8.4
IRAS 04374–6831				
9020.3		14.3	12.01	9.3
9295.3			12.24	
9745.3			12.4	9.6
10027.4		13.6	11.47	9.1
10034.5		13.7	11.41	9.0
10144.3		13.5	11.29	8.78
10326.5			12.20	
10388.6			12.57	
10500.4			12.7	
10765.4		13.7	11.34	
10915.2			11.85	9.0
11626.3			12.34	
IRAS 04496–6958				
9021.3	12.10	10.19	8.80	7.25
9115.2	12.42	10.43	8.98	7.45
9295.4	13.0	11.02	9.53	7.9
9353.3	13.06	11.12	9.61	8.0
9434.3	13.14	11.15	9.68	8.00
9495.2	12.82	10.84	9.39	7.82
9586.6	12.36	10.42	9.02	7.49
9701.4	12.08	10.20	8.80	7.3
9744.4	12.09	10.22	8.82	7.29
9791.3	12.23	10.31	8.91	7.35
9959.6	12.77	10.81	9.33	7.72
10029.4	13.05	11.03	9.53	7.89
10124.3	13.13	11.16	9.62	7.81
10324.6	12.22	10.34	8.91	7.50
10391.5	11.94	10.05	8.68	7.25
10446.4	11.95	10.04	8.68	7.30
10504.3	12.09	10.11	8.74	7.36
10856.3	12.93	10.96	9.47	7.8
11625.3	12.98	11.03	9.56	7.99
11888.5	11.89	10.05	8.73	7.23
11982.2	12.20	10.34	8.97	7.43
IRAS 04539–6821				
9021.4			12.19	9.14
9746.4			12.67	9.67
9961.6			13.1	
10031.4			12.9	
10147.3			11.88	
10327.5			11.98	9.05
10387.5			12.35	9.56
10500.4			13.1	
10764.5			12.4	9.44
IRAS 04557–6753				
9021.3		13.24	11.22	8.75
9116.2		13.47	11.23	8.69
9294.5			11.9	9.0
9298.6			11.96	

Table 1 – *continued*

JD –244 0000	*J*	*H*	*K*	*L*
		(mag)		
IRAS 04557–6753 continued				
9352.4		14.4	12.23	9.4
9434.3			12.4	
9701.5		13.6	11.47	
9745.3		13.6	11.30	8.8
9746.4		13.33	11.28	8.8
9791.4		13.4	11.25	8.7
9959.6		13.43	11.36	8.8
10028.4		13.7	11.66	9.0
10144.3		14.5	12.32	
10327.5			12.39	9.6
10500.4		13.4	11.19	8.9
11626.3			12.10	
IRAS 05009–6616				
9027.4	14.6	12.50	10.76	8.9
9296.4		13.3	11.59	
9352.4		13.3	11.46	9.1
9434.3		12.63	10.90	8.6
9495.2		12.39	10.61	8.37
9586.7		12.26	10.57	8.37
9701.5		12.90	11.12	8.8
9742.4		13.4	11.55	
9791.4		13.6	11.79	
9960.7		13.7	11.92	9.5
10027.4		13.6	11.75	9.2
10123.4		12.78	10.94	8.6
10325.5		12.83	11.06	8.6
10390.4		13.17	11.51	9.1
10475.3		13.9	12.0	
10500.5		13.7	12.04	
10764.5		12.96	11.04	8.6
10792.5		12.82	11.01	8.6
11210.4		14.4	12.57	
11480.5		13.2	11.14	8.56
11625.3		13.5	11.48	8.6
11888.5			12.75	
11988.4			12.53	9.5
IRAS 05112–6755				
9021.5			12.7	9.4
9297.3			13.2	
9747.4		14.3	12.07	8.9
10032.5			13.1	
10328.5		14.2	11.69	8.6
10387.5		14.0	11.55	8.5
10498.4		14.1	11.59	8.5
10764.5			13.0	9.6
IRAS 05113–6739				
9022.4			13.1	
9297.4			12.9	
9745.4			12.97	9.8
10032.4			12.5	
10328.5		14.2	12.05	9.0
10796.5		14.0	11.68	8.9
10915.3		13.8	11.43	8.56
IRAS 05128–6455				
9022.4	13.31	11.69	10.31	8.5
9116.2	13.44	11.92	10.52	8.74
9296.4		13.2	11.41	
9355.4		13.1	11.44	
9434.3		13.2	11.53	
9496.2		12.9	11.29	9.2
9701.6		11.86	10.36	8.4

Table 1 – *continued*

JD –244 0000	*J*	*H*	*K*	*L*
		(mag)		
IRAS 05128–6455 continued				
9742.4	13.51	11.80	10.38	8.42
9792.3	13.60	11.89	10.47	8.6
9938.7		12.32	10.87	9.1
10023.6		12.74	11.22	
10034.4	14.6	12.81	11.24	9.4
10126.5		13.14	11.48	
10325.6		12.37	10.75	8.65
10473.5		11.98	10.50	8.4
10917.2		12.72	10.99	
11625.3		12.90	11.29	
IRAS 05190–6748				
9057.3			12.18	8.6
9117.2			12.37	8.86
9297.4			13.3	9.8
9742.5			12.33	8.9
10031.5			12.00	8.8
10125.3			12.4	
10326.5			13.3	
10390.5			13.4	
10501.4			13.5	
10764.6			12.16	8.7
IRAS 05291–6700				
9021.5	12.8	11.02	9.93	8.8
9296.5	13.6	11.75	10.45	8.9
9355.4	13.02	11.47	10.30	8.9
9439.3	12.83	11.26	10.16	8.9
9495.2	12.59	11.05	10.01	8.62
9587.6	12.61	10.92	9.86	8.7
9702.4	13.49	11.69	10.38	9.0
9747.4	13.44	11.61	10.34	9.0
IRAS 05295–7121				
9023.3		12.88	11.03	9.0
9115.2	14.3	12.17	10.42	8.5
9296.6		12.32	10.49	8.4
9355.4		12.46	10.66	8.5
9439.3		13.1	11.18	9.1
9496.2		13.5	11.51	9.2
9702.5		13.2	11.14	8.9
9744.5		12.8	10.82	8.6
9792.4		12.49	10.63	8.5
9961.6		12.68	10.67	8.6
10027.5		13.27	11.08	8.9
10325.7		13.6	11.53	9.2
10390.5		13.07	11.00	8.7
10504.4		12.71	10.69	8.6
IRAS 05300–6651				
9023.4		13.8	11.58	9.0
9113.2		14.4	12.02	9.3
9297.5			13.0	
9745.5		14.3	11.72	8.6
10326.6		14.3	11.94	8.9
10501.5			12.17	
10797.5			13.4	
10915.3			12.33	
IRAS 05360–6648				
9026.5			13.0	
9300.6		13.7	12.41	9.4
9742.6			12.3	
10326.6			12.15	
10327.6			12.27	9.2

Table 1 – *continued*

JD –244 0000	*J*	*H*	*K*	*L*
		(mag)		
IRAS 05360–6648 continued				
10446.5			12.7	
10504.4			13.2	
SHV 05003-6817				
9748.3	14.2	12.17	10.84	
9960.6	12.92	11.27	10.15	9.0
10028.6	13.20	11.48	10.32	
10144.3	14.4	12.35	10.95	
10324.6	13.06	11.43	10.27	9.0
10355.6	13.06	11.38	10.22	
10383.5	13.17	11.46	10.26	8.9
10472.5	13.9	12.13	10.80	
SHV 05003–6829				
9748.3	13.06	11.25	9.91	8.4
9960.6	13.87	11.97	10.48	9.0
10031.5	14.0	11.98	10.56	9.0
10123.4	13.60	11.77	10.40	8.8
10323.6	13.15	11.35	10.07	8.6
10355.6	13.4	11.57	10.24	8.9
10382.6	13.6	11.78	10.40	
10443.5	14.1	12.20	10.73	
10474.4	14.2	12.23	10.74	9.2
SHV 05027–6924				
9748.3	12.96	11.66	10.98	
9960.7	12.49	11.15	10.60	
10028.5	13.03	11.70	10.89	
10144.4	12.41	11.38	10.87	
10324.6	12.97	11.65	10.89	
10355.6	12.96	11.69	10.97	
10498.3	12.19	11.09	10.71	
10915.3	12.98	11.59	10.87	
SHV 05210–6904				
9797.3	11.46	10.08	9.37	8.6
9963.6	11.72	10.50	9.74	
10031.5	11.55	10.33	9.68	8.9
10126.4	11.22	10.06	9.50	8.7
10320.7	11.35	9.98	9.32	8.7
10447.6	12.08	10.75	9.84	
10501.4	12.03	10.74	9.86	
10798.4	11.07	9.77	9.23	8.4
10887.3	11.49	10.08	9.39	8.8
10917.3	11.75	10.31	9.53	
11480.5	11.83	10.44	9.61	9.2
11623.2	11.82	10.64	9.75	
11888.5	10.92	9.67	9.06	8.3
SHV 05260–7011				
9963.6		12.37	10.90	
10031.6	13.9	12.06	10.72	9.4
10142.4	13.20	11.37	10.18	
10323.7		12.37	10.79	
10442.5	13.7	11.78	10.43	
10476.4	13.9	11.73	10.42	
10797.4	13.9	12.00	10.58	9.2
10887.3	13.22	11.52	10.29	9.1
10917.3	13.31	11.50	10.24	8.9
WBP 14				
9963.6	13.5	11.81	10.71	
10028.5	13.8	12.06	10.88	
10142.4	13.25	11.66	10.61	
10324.7	13.5	11.76	10.64	
10442.5	13.47	11.83	10.69	
10475.4	13.33	11.69	10.61	

Table 1 – *continued*

JD –244 0000	*J*	*H*	*K*	*L*
		(mag)		
WBP 14 continued				
10504.4	13.05	11.49	10.45	
10797.4	13.5	11.85	10.72	
10887.3	13.02	11.42	10.47	9.5
10915.3	12.96	11.39	10.40	9.3
TRM 72 (05116–6654)				
9027.4			10.50	
9058.2		12.55	10.67	8.34
9117.2		13.06	11.06	8.65
9295.5			11.96	
9352.4		13.41	11.52	9.1
9434.3		13.37	11.50	9.2
9587.6		12.61	10.86	8.5
9701.5		13.2	11.58	
9745.4		14.1	12.02	9.4
9792.3		14.4	12.38	
9938.7		14.0	11.95	9.3
10027.5		13.32	11.45	9.0
10122.4		13.07	11.07	8.5
10201.2		13.5	11.41	8.7
10325.4			12.28	9.4
10388.6			12.44	9.6
10501.4		14.2	11.90	
10764.6		12.65	10.89	8.6
10792.5		12.84	10.98	8.6
10915.3		13.7	11.52	9.3
11210.4	13.8	11.69	10.12	8.2
11480.5		12.99	11.21	9.1
11625.3		12.65	11.02	8.8
11888.5		12.40	10.67	8.6
11988.4		13.25	11.39	9.0
TRM 88 (05202–6638)				
9057.3		13.60	11.39	9.0
9117.2		13.07	11.13	9.0
9296.5		12.20	10.47	
9300.5		12.13	10.43	8.59
9352.4		12.16	10.40	8.5
9439.3		12.49	10.65	8.68
9702.4		12.01	10.40	8.7
9742.5	13.9	11.75	10.18	8.6
9792.3	13.11	11.24	9.83	8.3
9961.6	13.35	11.26	9.86	8.30
10027.5	13.7	11.59	10.14	8.5
10142.3	13.7	11.66	10.19	8.4
10201.2	13.4	11.45	10.06	8.6
10325.6	12.6	10.87	9.62	8.23
10390.6	12.44	10.71	9.46	8.05
10499.3	13.08	11.12	9.73	8.2
10764.6		11.77	10.25	8.6
10792.6	13.6	11.78	10.24	8.5
11210.4		13.0	11.23	
11625.3		13.2	11.34	9.0
11888.5		13.51	11.55	9.3
11988.4		12.62	10.82	8.7
Supergiants, SRs and others				
HV 5870				
4282.4	9.0	8.1	7.8	*
4552.5	9.3	8.43	8.06	*
4923.6	9.31	8.36	7.98	*
5012.4	9.34	8.41	8.05	*
5259.5	9.18	8.31	7.99	*
5649.5	9.34	8.47	8.17	*

Table 1 – *continued*

JD –244 0000	*J*	*H*	*K*	*L*
		(mag)		
HV 5870 continued				
5688.4	9.28	8.40	8.11	*
6031.4	9.53	8.63	8.24	*
6357.5	9.27	8.36	8.06	*
6381.6	9.23	8.34	8.04	*
6425.5	9.17	8.30	8.00	*
6489.4	9.19	8.31	7.97	*
6784.4	9.78	8.80	8.44	*
9705.4	9.26	8.32	7.97	7.48
9965.5	9.41	8.47	8.13	7.62
10033.5	9.39	8.47	8.14	7.62
10121.4	9.35	8.41	8.12	7.6
10323.7	9.12	8.18	7.85	7.34
10447.5	9.24	8.27	7.93	7.5
10501.5	9.35	8.39	8.01	7.47
10798.4	9.29	8.35	8.03	7.53
10858.5	9.34	8.39	8.03	7.6
IRAS 04530–6916				
9797.3	13.7	11.73	9.86	7.5
10032.5	13.6	11.58	9.71	7.5
10120.3	13.7	11.63	9.73	7.53
10317.6	13.5	11.49	9.74	
10392.4	13.80	11.62	9.74	7.72
10476.3	13.6	11.61	9.72	7.6
10764.5	13.9	11.79	9.94	7.74
10796.4	13.8	11.79	9.89	7.8
11097.5	13.76	11.71	9.79	7.63
IRAS 04553–6825 (WOH G064)				
9797.3	9.88	8.26	7.23	5.42
9960.6	9.83	8.25	7.24	5.45
10029.5	9.77	8.18	7.18	5.34
10144.2	9.64	8.06	7.05	5.18
10317.6	9.56	7.92	6.93	5.10
10446.4	9.60	7.98	6.99	5.19
10474.4	9.65	8.01	7.01	5.27
10761.5	9.80	8.22	7.25	5.48
10794.5	9.82	8.27	7.27	5.50
10917.3	9.69	8.12	7.11	5.24
IRAS 04559–6931 (HV 12501)				
9705.3	8.70	7.88	7.67	7.32
9747.4	8.72	7.87	7.66	7.24
9959.7	8.71	7.89	7.63	7.25
10031.4	8.77	7.92	7.67	7.31
10120.3	8.88	8.04	7.77	7.36
10325.7	8.79	7.95	7.73	7.37
10392.5	8.78	7.95	7.69	7.43
10472.5	8.74	7.94	7.70	7.32
IRAS 05042–6720 (HV 888)				
4941.5	7.86	7.03	6.78	
5016.3	7.74	6.94	6.68	6.3
5705.3	7.99	7.20	6.88	*
6066.5	7.99	7.10	6.78	6.36
6358.5	8.06	7.21	6.91	*
6425.3	8.07	7.22	6.92	*
6444.4	8.06	7.21	6.91	*
6489.4	8.04	7.21	6.89	*
6784.4	7.86	6.99	6.68	*
9705.3	7.97	7.06	6.78	6.38
9960.7	8.09	7.15	6.85	6.40
10031.6	8.10	7.19	6.88	6.44
10124.3	8.10	7.21	6.89	6.4
10325.6	8.10	7.18	6.89	6.48

Table 1 – *continued*

JD –244 0000	*J*	*H*	*K*	*L*
		(mag)		
IRAS 05042–6720 (HV 888) continued				
10476.4	8.00	7.08	6.79	6.37
11834.6	7.78	6.89	6.60	6.16
IRAS 05128–6723 (HV 2360)				
4922.5	8.88	8.02	7.67	*
5677.4	8.85	7.97	7.64	*
6066.5	8.82	7.96	7.56	6.96
6357.5	8.83	7.94	7.57	*
6428.4	8.78	7.93	7.58	*
6490.4	8.77	7.90	7.57	*
6787.4	8.77	7.92	7.60	*
9705.4	8.88	8.02	7.66	7.15
9963.6	8.98	8.08	7.72	7.06
10028.4	9.00	8.11	7.76	7.14
10144.4	9.08	8.19	7.82	7.25
10325.6	8.87	8.02	7.70	7.12
10353.6	8.86	8.01	7.69	7.18
10390.6	8.84	8.01	7.67	7.12
10473.4	8.92	8.06	7.71	7.24
IRAS 05148–6730 (HV 916)				
4920.6	8.84	7.91	7.57	*
5020.3	8.16	7.76	7.48	*
5680.4	8.71	7.80	7.47	*
6031.3	8.68	7.73	7.43	*
6113.3	8.68	7.76	7.46	*
6357.6	8.53	7.62	7.33	*
6427.4	8.62	7.67	7.38	*
6491.3	8.65	7.74	7.43	*
6798.5	8.78	7.81	7.49	*
9705.4	8.70	7.79	7.47	7.01
9961.6	8.58	7.65	7.36	6.93
10032.4	8.53	7.57	7.29	6.86
10122.4	8.41	7.51	7.22	6.77
10324.7	8.69	7.75	7.42	6.93
10447.5	8.75	7.84	7.53	7.03
10504.3	8.80	7.89	7.57	7.15
10762.6	8.71	7.79	7.51	7.06
10917.3	8.58	7.64	7.37	6.94
IRAS 05316–6604				
9965.5	10.15	9.28	8.78	7.81
10028.5	10.12	9.28	8.76	7.77
10142.4	10.29	9.47	8.95	8.0
10323.6	10.60	9.77	9.16	8.2
10353.6	10.68	9.82	9.19	8.2
10442.5	10.42	9.56	8.98	8.0
10475.4	10.28	9.44	8.91	
10504.4	10.22	9.41	8.90	8.0
10798.4	9.90	9.10	8.64	7.69
10887.4	10.13	9.36	8.87	7.90
10915.3	10.20	9.41	8.89	7.96
11210.5	10.57	9.70	9.14	8.2
IRAS 05327–6757 (HV 996)				
6357.5	9.17	8.23	7.69	*
6428.5	9.06	8.14	7.67	*
6490.4	8.98	8.09	7.63	*
6801.5	8.84	7.94	7.51	*
9705.3	8.91	7.95	7.49	6.76
9746.6	8.97	8.00	7.51	6.76
10029.5	8.98	8.07	7.64	6.83
10123.3	8.94	8.04	7.59	6.83
10317.6	8.94	7.99	7.56	6.86
10447.5	8.99	8.05	7.62	6.91
10476.3	9.02	8.06	7.61	6.91

Table 1 – *continued*

JD –244 0000	*J*	*H*	*K*	*L*
		(mag)		
SHV 05221–7025				
9963.6	13.6	11.99	10.83	
10032.5	14.4	12.63	11.17	
10327.6	12.97	11.46	10.41	
10499.4	13.92	12.22	10.98	
10704.6	13.4	11.88	10.76	
10796.5	14.4	12.78	11.35	
10889.3	14.5	12.49	11.32	
10917.2	14.6	12.68	11.29	
SHV 05357–7024				
9746.5	12.03	11.03	10.76	
10029.6	12.08	11.01	10.76	
10142.5	12.14	11.12	10.94	
10201.3	12.06	10.99	10.76	
10201.3	12.58	11.27	10.46	
10323.7	13.26	11.70	10.75	
10442.5	12.59	11.28	10.52	
10473.4	12.58	11.21	10.50	
10498.5	12.53	11.22	10.45	
10887.4	12.88	11.48	10.62	
10914.2	13.11	11.62	10.72	
11890.5	13.84	12.13	11.05	
11982.3	13.35	11.84	10.85	
GRV 0519430–670044				
9797.3	12.94	11.59	10.79	
9961.6	12.10	11.01	10.58	
10027.6	12.79	11.57	10.81	
10144.4	13.11	11.71	10.89	
10324.6	12.63	11.35	10.67	
10442.5	12.93	11.63	10.86	
10474.5	12.97	11.64	10.91	
10504.3	12.83	11.61	10.93	
10767.5	12.96	11.66	10.91	
10797.4	12.85	11.61	10.94	
10887.3	12.23	11.06	10.61	
10915.3	12.28	11.08	10.57	
11890.6	12.74	11.36	10.62	
11949.4	13.05	11.71	10.85	
GRV 0519486–645415				
10387.6	12.98	11.80	11.20	
10442.4	12.59	11.41	10.97	
10470.5	12.87	11.64	11.03	
10498.3	13.29	11.98	11.26	
10602.2	13.18	11.99	11.33	
10701.6	12.65	11.48	10.97	
10761.5	13.2	12.00	11.24	
GRV 0530506–643714				
10443.4	13.5	12.78	12.60	
10471.4	12.9	12.06	11.81	
10498.4	12.72	11.85	11.54	
10602.2	12.94	12.14	11.87	
10706.6	13.5	12.45	11.95	
10762.6	13.11	12.46	12.5	
GRV 0537140–674024				
10387.6	12.98	11.47	10.45	9.6
10442.4	12.09	10.75	10.07	
10471.5	12.76	11.33	10.39	
10498.4	12.05	10.70	10.01	
10760.6	11.96	10.56	9.89	
10762.5	11.96	10.55	9.88	8.8
IRAS 05289–6617				
11181.5	14.2	13.22	12.70	

Table 2. Mean magnitudes, amplitudes and periods for the LMC sources.

Name	J	H	K	L	n	ΔJ	ΔH	ΔK	ΔL	P_K	$P_{\rm other}$	note
O-rich AGB stars												
HV 12070	10.43	9.48	9.04	8.4	21	0.88	1.02	0.88	0.8	623	621	3,HBB
HV 2446	10.49	9.50	9.06	8.4	16	0.73	0.87	0.77	0.6	596	600	4
IRAS 04407–7000	11.13	9.67	8.79	7.62	27	1.67	1.53	1.23	1.08	1199		
IRAS 04498–6842	9.94	8.87	8.08	7.16	20	1.82	1.66	1.30	1.23	1292		
IRAS 04509–6922	10.80	9.42	8.59	7.56	25	2.01	1.82	1.45	1.19	1292	1290	1
IRAS 04516–6902	11.04	9.55	8.72	7.67	21	1.76	1.71	1.41	1.38	1091	1090	1
IRAS 04545–7000		12.57	10.13	7.84	28		1.81	1.57	1.45	*1216	1270	1
IRAS 05003–6712	12.90	11.26	9.95	8.49	12	1.97	1.92	1.59	1.44	883		
IRAS 05294–7104	12.18	10.33	9.21	7.94	16	1.8	1.5	1.2	1.2	1079	1040	1
IRAS 05329–6708		12.7	9.9	7.6	43		2.2	1.5	1.5	1262	1295	2,W
IRAS 05402–6956			10.4	8.0	21			1.8	1.4	1393	1390	1
IRAS 05558–7000	12.52	10.50	9.25	7.82	16	1.85	1.71	1.42	1.32	1220		
SHV 04544–6848	10.72	9.69	9.13	8.36	7	1.21	1.18	0.97	0.8	645	728	5
SHV 05220–7012	13.02	12.06	11.73		7	0.85	0.9	0.74		219	204	5
SHV 05249–6945	12.14	10.92	10.39		6	1.1	0.9	0.8		425	413	5
SHV 05305–7022	11.96	11.00	10.57		8	0.60	0.75	0.68		362	348	5
R105	11.75	10.74	10.33		20	0.70	0.70	0.63		413	420	6
WBP 74	12.83	11.87	11.50		16	0.53	0.51	0.48		245	227	8
GRV 0517584–655140	13.39	12.56	12.25		15	0.58	0.54	0.46		116	117	6
RHV 0524173–660913	11.04	10.09	9.69		10	0.79	0.89	0.81		490	486	5
C-rich AGB stars												
IRAS 04286–6937	15.0	12.77	10.95	8.82	13		1.28	1.13	1.03	662		
IRAS 04374–6831		14.20	11.96	9.26	9			1.44		639		
IRAS 04496–6958	12.57	10.63	9.18	7.62	19	1.07	1.00	0.88	0.67	723		HBB
IRAS 04539–6821			12.51		9			1.65		676		
IRAS 04557–6753		13.93	11.78	9.11	16		1.42	1.36	0.93	765		
IRAS 05009–6616		13.06	11.29	8.94	23		1.5	1.5	1.4	*658		
IRAS 05112–6755		15.1	12.39	9.13	27			1.75	1.35	830	822	2,W
IRAS 05113–6739		14.6	12.39	9.1	27			1.82		700	713	2,W
IRAS 05128–6455	14.1	12.46	10.91	9.0	17	1.3	1.28	1.06	1.0	708		
IRAS 05190–6748			12.82		29			1.66		939	889	2
IRAS 05291–6700	13.04	11.33	10.17	8.86	8	0.87	0.74	0.52	0.24	483		
IRAS 05295–7121		12.96	10.99	8.83	14		1.28	1.15	0.92	682		
IRAS 05300–6651		14.8	12.30		27			1.62		*708	683	2,W
IRAS 05360–6648			12.91		27			1.22		538	530	2
SHV 05003–6817	13.70	11.85	10.58	9.3	8	1.4	1.0	0.77		369	396	5
SHV 05003–6829	13.65	11.74	10.33	8.8	9	1.26	1.06	0.88		441	477	5
SHV 05027–6924	12.59	11.40	10.82		8	0.80	0.67	0.42		298	310	5
SHV 05210–6904	11.44	10.18	9.50	8.8	13	1.07	0.99	0.65	0.8	541	524	5, HBB
SHV 05260–7011	13.6	11.92	10.54		9	0.8	0.89	0.62		373	436	5
WBP 14	13.35	11.70	10.62		10	0.79	0.63	0.42		351	325	8
TRM 72		13.1	11.2	8.9	25		1.4	1.3	1.0	*571	631	2
TRM 88	13.4	11.43	9.99	8.38	22	1.0	0.93	0.71	0.42	*544	565	2
Supergiants, semiregular and irregular variables, or insufficient data												
HV 5870	9.41	8.32	7.99	7.48	20	0.2	0.2	0.2	0.2	320	627?	3,4
IRAS 04530–6916	13.75	11.69	9.82	7.67	9	0.2	0.2	0.2	0.3	none	1260:	1
IRAS 04553–6825	9.69	8.09	7.09	5.28	10	0.32	0.35	0.34	0.42	841	930	1
IRAS 04559–6931	8.79	7.97	7.70	7.30	8	0.2	0.1	0.1	0.1	none	675	
IRAS 05042–6720	7.99	7.12	6.82	6.38	16	0.2	0.2	0.2	0.2	none	850	
IRAS 05128–6723	8.95	8.07	7.69	7.11	15	0.3	0.3	0.3	0.3	none	409	
IRAS 05148–6730	8.66	7.77	7.43	6.97	17	0.28	0.28	0.24	0.28	951	743	
IRAS 05316–6604	10.29	9.46	8.92	7.94	12	0.8	0.7	0.6	0.5	none		
IRAS 05327–6757	8.97	8.04	7.59	6.8	11	0.2	0.2	0.2	0.1	595	760	5
SHV 05221–7025	13.8	12.11	10.93		8	1.5	1.26	0.82			384:	5,S?
SHV 05357–7024	12.89	11.46	10.60		5	>0.7	>0.5	>0.3		none		
GRV 0519430–670044	12.70	11.44	10.77		14	0.82	0.62	0.30		312	314	7
GRV 0519486–645415	12.87	11.74	11.13		17	0.69	0.61	0.33		236	242	6
GRV 0530506–643714	13.12	12.42	12.08		18	1.3	1.2	1.1		157	157	7
GRV 0537140–674024					15					odd	418	6
IRAS 05289–6617	14.20	13.22	12.70		1							

Notes to Table 2: HBB: these objects are thought to be, or have recently been, undergoing HBB. W: the mean H magnitude was estimated using data from Wood et al. (1992) and/or Wood (1998). S?: possibly S spectral type (Hughes & Wood 1990). References for $P_{\rm other}$: (1) Wood et al. (1992), (2) Wood (1998), (3) Gaposchkin (1970), (4) Payne-Gaposchkin (1971), (5) Hughes & Wood (1990), (6) Feast et al. (1989), (7) Reid, Glass & Catchpole (1988), (8) Wood, Bessell & Paltoglou (1985).

bolometric magnitudes brighter than the tip of the AGB, i.e. $M_{\rm bol} < -7.2$ mag. The other 10 stars are semiregular or irregular variables or stars without sufficient data to classify them properly (it is possible that the measurements of some of these stars were contaminated by the proximity of other IR sources). The following discussion is limited to regular AGB variables, i.e. leaving out the supergiants, etc.

The pulsation periods (P_K), listed in Table 2, were determined from Fourier transforms of the K light curves. Data from Glass et al. (1990) were used in addition to that given in Table 1, while for stars in common with Wood et al. (1992) and/or Wood (1998) the combined K data sets, which provide very well-sampled light curves, were used for period determination. The results are generally in good agreement with values determined by others ($P_{\rm other}$) except for the semiregular and irregular variables where the agreement is often rather poor. Among the large-amplitude variables, our data for SHV 05260–7011 does not fit the 436-d period determined by Hughes & Wood (1990).

In the case of one O- and four C-rich stars the light curves show very long-period or secular changes in addition to the obvious periodic variations from pulsation. The periodicity of these long-term trends is very uncertain and would require many more years of measurement to characterize. The long-term trends are discussed further in Section 4. The peak-to-peak amplitudes of the best-fitting sine curves, given in Table 2, refer only to the periodic pulsations and the full variation of those stars with long-term trends can be much larger than the values tabulated. A few of the very long-period O-rich stars have rather asymmetric light curves and the tabulated amplitudes of the best-fitting sine curves therefore represent lower limits to the true peak-to-peak variations.

The mean magnitudes are determined from the Fourier fitted sine curves. In the case of stars with a long-term trend the mean used is that of the brightest cycles. As these means are used to determine the bolometric magnitudes, this procedure might lead to an overestimate of the total flux, depending on what is causing the long-term changes.

Fourier mean intensities are brighter than the mean magnitudes quoted here by up to 0.3 mag at K, although for most stars the differences are around $\Delta K \sim 0.1$ mag. The difference in bolometric magnitudes estimated via intensity means is much smaller (see below).

Fig. 3 shows a range of amplitudes at a given period, with the amplitudes of the longer-period C stars tending to be larger than those of their O-rich counterparts, possibly because the C-star temperatures are lower and therefore a steeper part of the blackbody light-curve is sampled at these near-infrared wavelengths. The bolometric amplitudes may show much less spread than do these ΔK values, but our information on them is very limited. At a given period the stars with the larger K amplitudes do tend to have redder colours and higher mass-loss rates, as would be expected if pulsation is driving the mass loss; compare, for example, the two C stars IRAS 05113–6739 and 05128–6455, both of which have periods around 700 d, but pulsation amplitudes of $\Delta K \sim 1.8$ and 1.1 mag, colours $K - [12] \sim 7.3$ and 5.7 and mass-loss rates $\dot{M} \sim 1.1 \times 10^{-5}$ and 0.6×10^{-5} $\mathrm{M}_{\odot}$ yr^{-1}, respectively (see Table 3). In general, the amplitudes of these AGB stars are comparable to those found by Olivier, Whitelock & Marang (2001) among galactic O- and C-rich stars with similar periods. The HBB stars all have rather low amplitudes for their period, although not outside the range of the others.

In a plot of $K - [12]$ against period or amplitude (see, e.g., Figs 4 and 5) there is a clear separation of the O- and C-rich stars, although it is interesting to note that the C-rich HBB stars fall with O-rich stars rather than with the other C stars. The separation between C and O types is also clear in the near-infrared colours as illustrated in Figs 6 and 7.

4 LONG-TERM TRENDS

The K light curves that show clear long-term trends are illustrated in Figs 8–12. The curves fitted to the data are described in the captions; all of them comprise two periods, the main pulsation period as listed in Table 2 and a significantly longer period chosen to represent the long-term trend.

For IRAS 04545–7000, the only O-rich star that shows a trend, a harmonic is also used to provide a much better fit to its distinctly asymmetric light curve. For the four carbon stars a simple sinusoid provides a very good fit to the main pulsational variation.

The time base is far too short to establish the periodicity, if any, of these long-term trends. Indeed, it is only for TRM 72 and TRM 88 that we have any real indication that the trends might by cyclical, and in these two stars periods of $5P_K$ and $6P_K$, respectively, were used to fit the trends. However, these long periods are not well constrained and significantly different periods could provide equally good fits to the trends.

The amplitudes of the trends are large, ranging from at least 0.5 up to about 1.0 mag at K, i.e. comparable to the main pulsation amplitude. The data at other wavelengths are not so extensive, but they are adequate to show that trend amplitudes are wavelength dependent in roughly the same way as the pulsation amplitudes, i.e. greater at shorter wavelengths.

Long-term trends and erratic or secular variations have been observed in various long-period variables and seem to be more prevalent among C stars than O-rich stars. In the case of V Hya the $\Delta K \sim 1.7$ mag variations over a 6160-d cycle (e.g. Olivier et al. 2001 and references therein), are best explained as the result of orbital variations in a binary system. In several other galactic C stars, most notably R For, the long-term changes are erratic and best interpreted as the result of mass-loss variations (e.g. Whitelock et al. 1997), possibly akin to R CrB variations that are caused by the ejection of 'soot' clouds in random directions.

Winters et al. (1994) have predicted periodic mass-loss variations on time-scales of a few times the pulsation period. It seems likely that the trends described here are caused by mass-loss variations, but only very long-term monitoring will characterize them sufficiently well to see if they fit the Winters et al. model.

5 *IRAS* FLUXES

The *IRAS* fluxes for most of these sources are listed in table 3 of Paper V where a comparison is also made with the fluxes measured by *ISO*. We use only the 12- and 25-μm flux here, noting the high uncertainty of measurements at longer wavelengths. The fluxes were colour-corrected only for the purpose of estimating the bolometric magnitudes. Thus for the various figures the *IRAS* magnitudes were calculated from: $[12] = \log 28.3/F_{12}$ and $[25] = \log 6.73/F_{25}$, for comparison with other papers in this series, but we note that this process differs from that used by Olivier et al. (2001), for example, who colour-correct the *IRAS* data used throughout their discussion.

6 BOLOMETRIC MAGNITUDES

Bolometric magnitudes, listed in Table 3, were calculated by integrating under a spline curve fitted to the mean J_{74}, H, K, L, 12- and

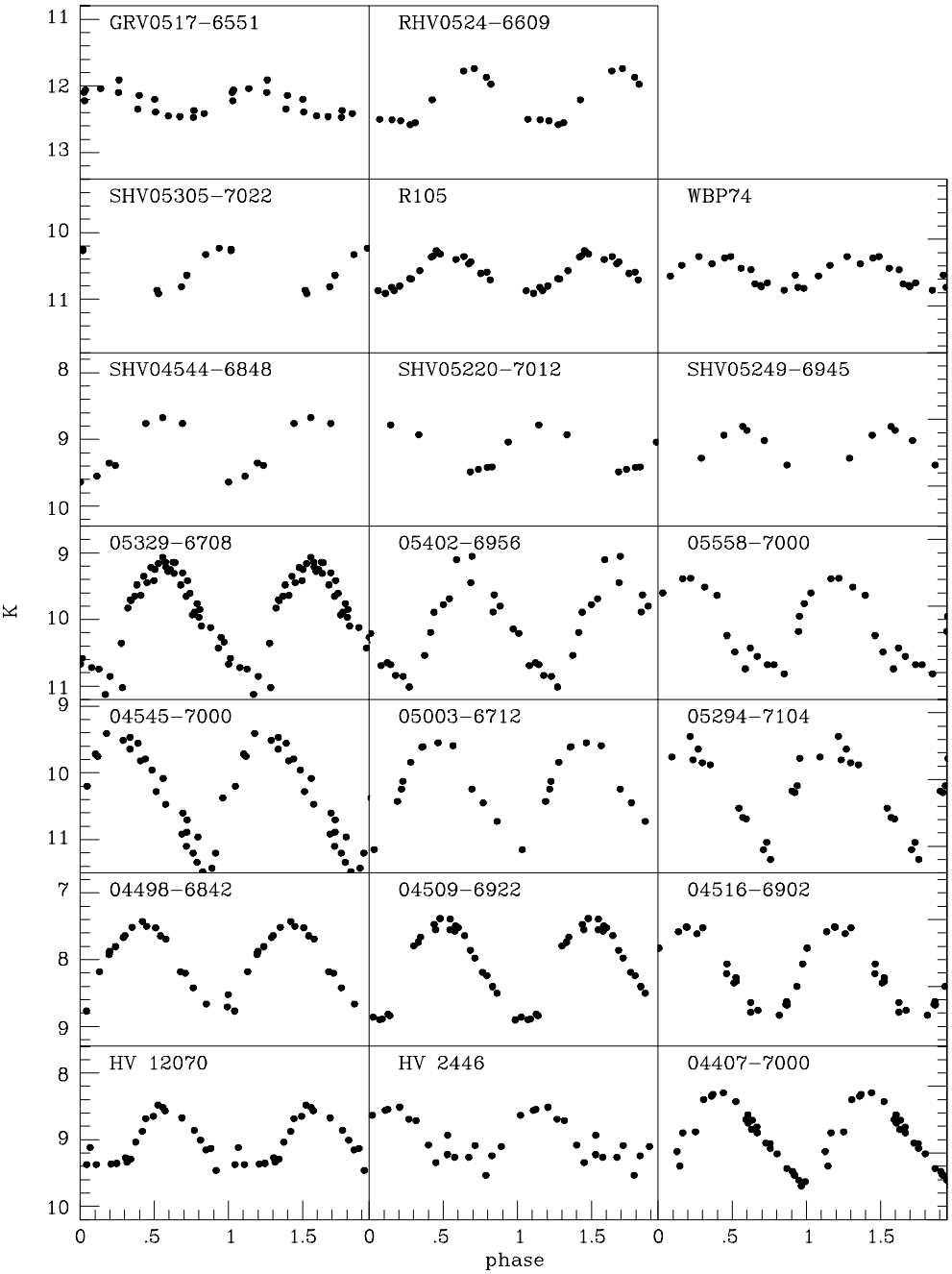

Figure 1. *K* light-curves for the O-rich AGB variables; each point is plotted twice to emphasize the variability and the full height of each box is 2.6 mag. The phase is arbitrary (JD2 440 000 is phase zero in all cases) and uses the period of P_K from Table 2.

25-μm fluxes as a function of frequency, following the procedure described in Section 6 of Whitelock et al. (1994).

The *HKL* values used are those listed in Table 2. The *J* magnitude was converted back to the 74-in system for consistency with Feast et al. (1989); in fact, the *J* flux is negligible for almost all of these stars so the conversion makes no practical difference. The 12- and 25-μm *IRAS* fluxes (see Section 5) were colour-corrected using the 12- to 25-μm flux ratio, as described in the explanatory supplement of the PSC.

In cases where there was no magnitude available for particular wavebands the following procedures were adopted for estimating a value to use in the integration (based on relationships deduced from sources measured in all the relevant bands).

For O-rich stars

For the one star, SHV 05402–6956, with no *H* magnitude we use equation (3) from Paper IV to derive $(H - K)$ from $K - [12]$.

For the eight stars without *L* measures, the expression $(K - L) = 0.239 + 0.946(H - K)$, which was derived from a least-squares fit to the colours of the other O-rich stars, was used to derive $(K - L)$ from $(H - K)$. This assumption is important only for SHV 05221–7025, which is moderately red with $(H - K) = 1.18$ and thus $(K - L) = 1.36$; the others all have $(K - L) < 0.75$.

For the four stars without *IRAS* 12-μm fluxes and the three with upper limits only, we use equation (3) from Paper IV to derive

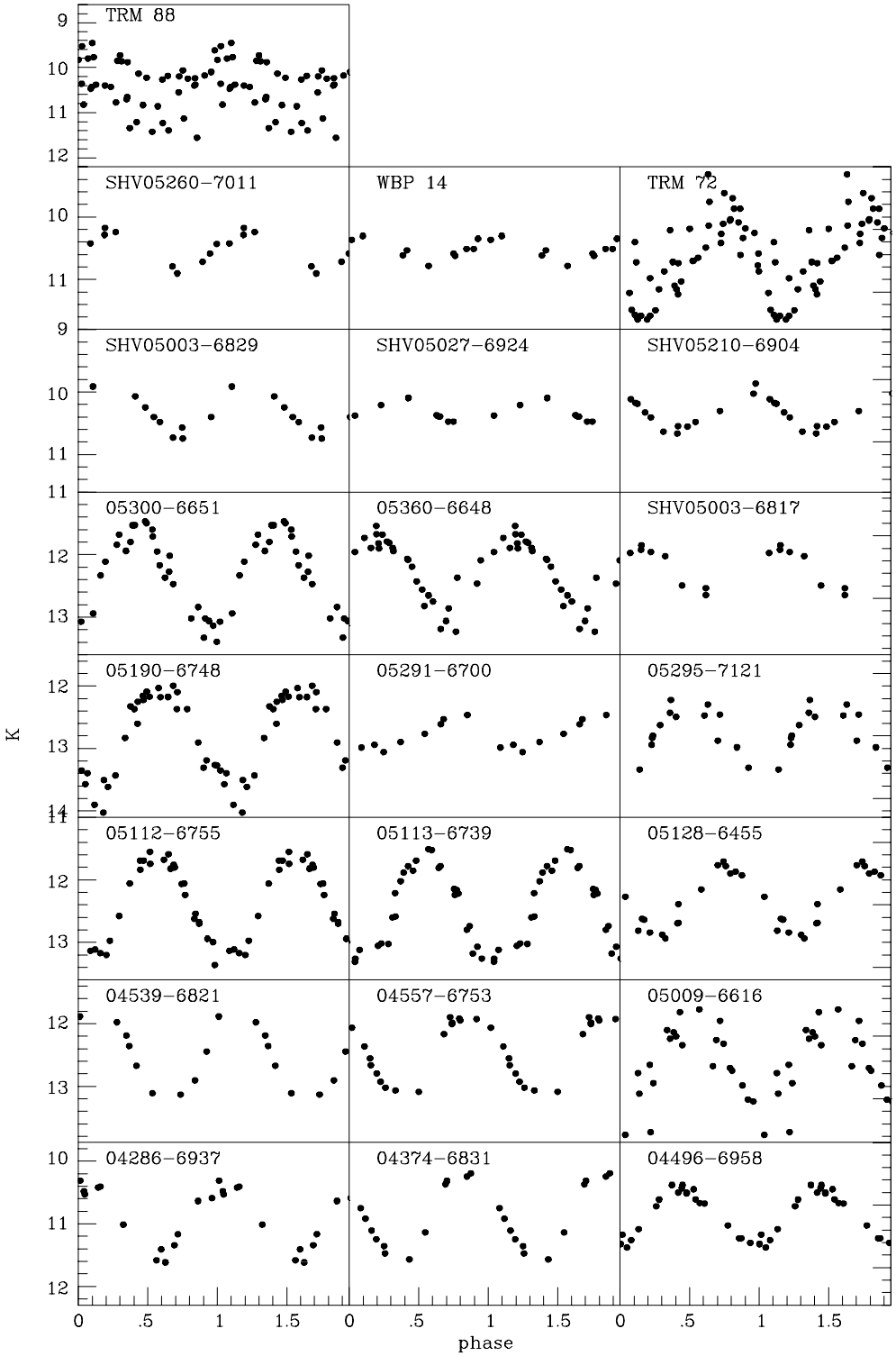

Figure 2. *K* light-curves for the C-rich AGB variables (see Table 2 for details).

$K - [12]$ from $(H - K)$. Stars without 25-μm fluxes are assumed to have uncorrected [12]−[25] = 0.9 mag.

For the C-rich stars

For three stars without H magnitudes we use equation (2) of Paper IV to derive $(H - K)$ from $K - [12]$.

For six stars without L magnitudes, L is estimated from [12] via $K - [12] = 1.737 + 1.838(K - L)$, a relation derived from a least-squares fit to the other C stars. For WBP14, $(K - L) = 0.4$ is assumed as its *IRAS* flux is anomalously faint.

Only one star has no 12-μm flux, IRAS 05291–6700, and this is estimated from equation (2) of Paper IV. The three stars without 25-μm fluxes are assumed to have [12]–[25] = 0.

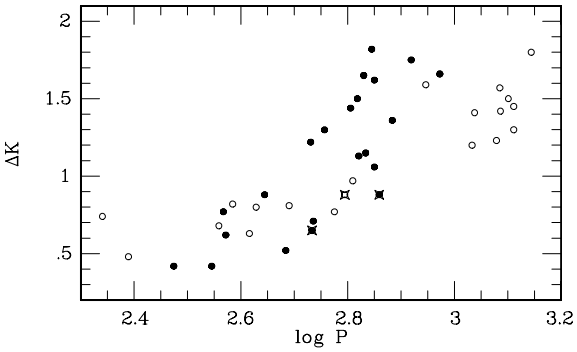

Figure 3. The pulsation amplitude at K, ΔK, as a function of the period, P; solid and open symbols are C- and O-rich stars, respectively, while HBB sources are starred.

In all cases without a J measure, O- or C-rich, the relation $(J - H) = 1.4(H - K)$ is assumed to derive it.

Because it is only the stars that have most of their flux at long wavelengths that lack J or H measures, and vice versa, most of these estimates of the missing quantities have little effect on the derived bolometric luminosity. Thus it is only the assumptions concerning the L magnitudes that are potentially important for the bolometric magnitude.

A comparison of Fourier mean magnitudes and intensities for the *JHKL* observations, indicates that the effect of using intensity means rather than magnitude means is to brighten the bolometric magnitude by between 0.01 and 0.06 mag. Using intensities would therefore have a negligible affect on the discussion and conclusions of this paper. Bolometric amplitudes are discussed briefly in Section 7.1.

6.1 Bolometric correction

Fig. 13 shows the bolometric correction to K as a function of various colours. It is illustrated here because it is potentially useful for application to other stars. The $(K - L)$ and $(H - K)$ relationships are distinctly different for O- and C-rich stars. For $K -$ [12], the relationship is very similar for the two types, at least for the redder colours. Note that, because the bolometric magnitude is determined by integrating under the flux curve as a function of frequency, the bolometric correction is not independent of the colours against which it is plotted.

6.2 Comparison with Feast et al. (1989)

Feast et al. established PL relations from 29 O-rich and 20 C-rich LMC Miras after deriving bolometric magnitudes by fitting blackbodies to fluxes from mean *JHK* photometry – all that was available at the time.

Fitting blackbodies is an effective way of deriving bolometric magnitudes if the dust shells make a negligible contribution to the total luminosities, as they do for most short period Miras. It is obviously important to look for any systematic differences in the blackbody and spline-fitting methods of establishing total luminosity. For this purpose we use both methods to estimate the total flux for sources with $P < 441$ d and make a comparison in Table 4.

The O-rich stars used by Feast et al. (1989) to establish the PL relation all have $(J - K) < 1.5$ mag. The six O-rich stars in Table 4 with $(J - K) < 1.5$ mag have bolometric and spline luminosities that agree to better than 0.2 mag, five out of six agree to better than 0.04 mag. SHV 05221–7025 shows a slightly brighter $m_{\rm bol}$ from the spline fit as would be expected for a stronger dust shell contribution. Note, however, that SHV 05221–7025 (which is classed among the semiregulars in Table 2) is the only source in this sample that has an *IRAS* flux measurement, whereas the others were all estimated from the near-IR colours.

The C-rich stars used by Feast et al. (1989) to establish the PL relation all have $(J - K) < 3$ mag. Stars with similar colours in this sample have spline- and blackbody-fitting magnitudes that agree to better than 0.2 mag (except for WBP 14, see Section 6 and Paper V, fig. 2, where the ratio of the *ISO* to revised-*IRAS* flux for WBP 14 is 2.2 – the largest value found). The redder stars tend to have slightly

Table 3. Absolute bolometric magnitudes derived using *IRAS* data (where available).

Name	$M_{\rm bol}$	$K - [12]$ (mag)	$\log(\dot{M})$
O-rich			
HV 12070	−6.48	2.36	−6.30
HV 2446	−6.40	2.18	−5.82
IRAS 04407–7000	−7.11	4.87	−4.30
IRAS 04498–6842	−7.72	4.76	−4.59
IRAS 04509–6922	−7.28	4.83	−4.77
IRAS 04516–6902	−7.11	4.93	−4.48
IRAS 04545–7000	−6.56	5.66	−3.55
IRAS 05003–6712	−6.20	5.40	−4.54
IRAS 05294–7104	−6.79	5.18	−4.19
IRAS 05329–6708	−6.95	5.94	−3.74
IRAS 05402–6956	−6.77	6.40	−3.74
IRAS 05558–7000	−6.97	5.44	−4.30
SHV 04544–6848	−6.45	3.90	
SHV 05220–7012	−3.87		<-8.00
SHV 05249–6945	−4.97		−6.70
SHV 05305–7022	−4.97		−6.40
R105	−5.16		
WBP 74	−4.07		
GRV 0517584–655140	−3.67		
RHV 0524173–660913	−5.88		
C-rich			
IRAS 04286–6937	−5.66	5.94	−5.30
IRAS 04374–6831	−5.25	6.78	−5.10
IRAS 04496–6958	−6.42	4.28	−5.25
IRAS 04539–6821	−5.13	7.24	−5.00
IRAS 04557–6753	−5.35	6.60	−5.10
IRAS 05009–6616	−5.50	6.28	−5.10
IRAS 05112–6755	−5.92	7.91	−4.85
IRAS 05113–6739	−5.34	7.26	−4.96
IRAS 05128–6455	−5.58	5.69	−5.22
IRAS 05190–6748	−5.69	8.17	−4.72
IRAS 05291–6700	−5.16		
IRAS 05295–7121	−5.35	5.76	−5.22
IRAS 05300–6651	−5.41	7.29	−4.96
IRAS 05360–6648	−4.96	7.59	−5.05
SHV 05003–6817	−5.05	4.55	−5.72
SHV 05003–6829	−5.15	4.20	−5.80
SHV 05027–6924	−4.44	2.94	<-8.00
SHV 05210–6904	−5.70	2.82	−6.22
SHV 05260–7011	−4.76	4.02	−6.10
WBP 14	−4.19	1.99	−6.30
TRM 72	−5.22	5.93	−5.30
TRM 88	−5.56	4.44	−5.52

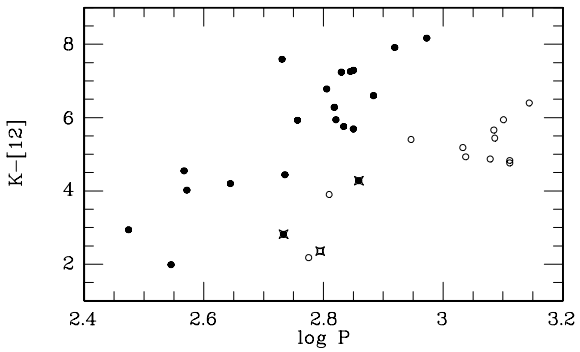

Figure 4. The $K - [12]$ colour as a function of the period, P; solid and open symbols are C- and O-rich stars, respectively, while HBB sources are starred.

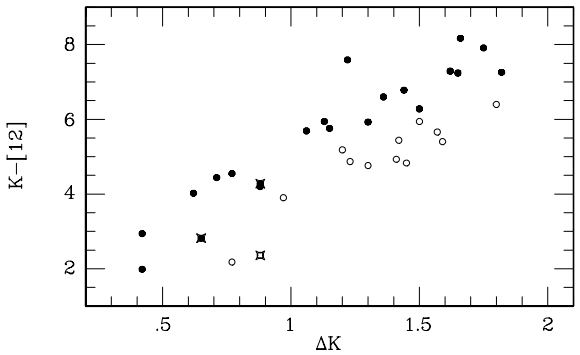

Figure 5. The $K - [12]$ colour as a function of the pulsation amplitude at K, ΔK; solid and open symbols are C- and O-rich stars, respectively, while HBB sources are starred.

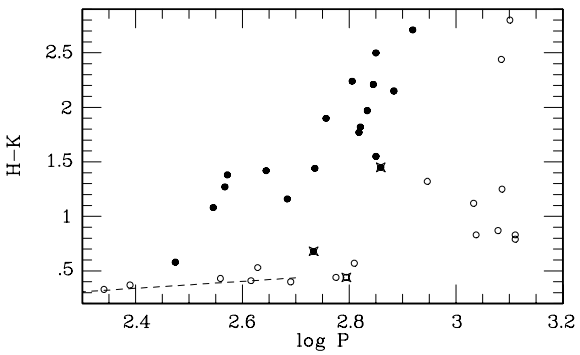

Figure 6. The $(H - K)$ colour as a function of the period, P; solid and open symbols are C- and O-rich stars, respectively, while HBB sources are starred. The line is the period-colour relation for O-rich Miras in the LMC with $P < 420$ d, from Feast et al. (1989).

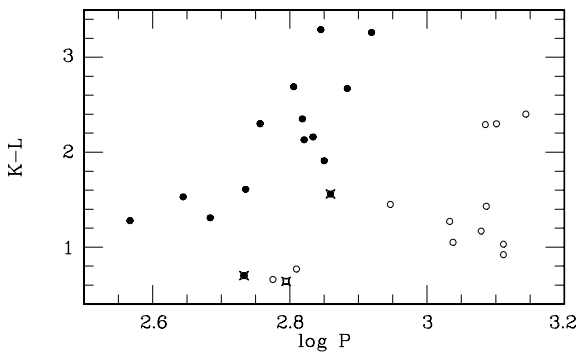

Figure 7. The $(K - L)$ colour as a function of the period, P; solid and open symbols are C- and O-rich stars, respectively, while HBB sources are starred.

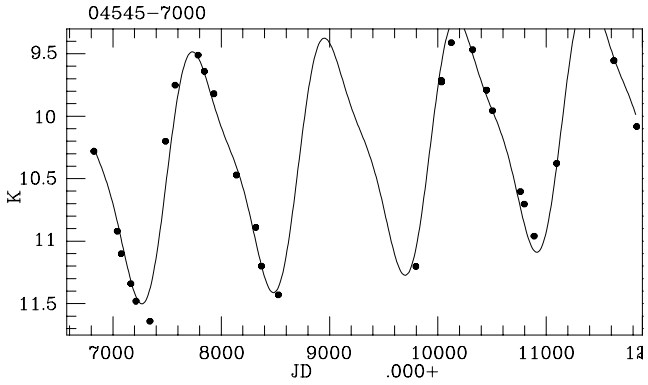

Figure 8. The K light curve for IRAS 04545–7000, including data from Wood et al. (1992). The curve is a 1216-d sinusoid with first harmonic and long-term trend (illustrated using a 50 000-d sinusoid).

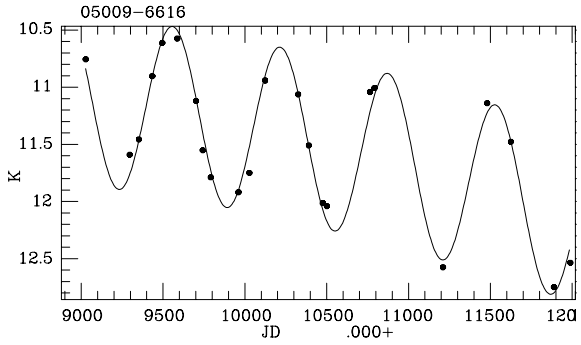

Figure 9. The K light curve for IRAS 05009–6616. The curve is a 658-d sinusoid with a long-term trend (illustrated using a 100 000-d sinusoid).

brighter spline-fitting magnitudes. In this case all but one of the stars have measured *IRAS* fluxes.

In summary, blackbody- and spline-fitting bolometric magnitudes agree to better than 0.2 mag (usually better than 0.1 mag) for O-rich stars with $(J - K) < 1.5$ mag and for C-rich stars with $(J - K) < 3$ mag. For stars with larger values of $(J - K)$ the blackbody method probably underestimates the total flux.

7 PL RELATION

Fig. 14 illustrates the PL relation ($M_{\rm bol}$ calculated from *IRAS* fluxes) for the stars under discussion and compares them with extrapolations of the PL relations derived by Feast et al. (1989) for stars with periods under 420 d. The PL relation derived by Groenewegen & Whitelock (1996) for C stars goes approximately through the middle of the two lines from Feast et al. and would fit these C-star luminosities rather well. WBP 14 is not illustrated in Fig. 14 as there are reasons to think its *IRAS* flux is too faint. It is, however, illustrated in the *IRAS*/*ISO* comparison made below (Fig. 15).

Nishida et al. (2000) discuss the luminosities and periods of three newly discovered C-rich Miras in Magellanic Cloud clusters. The two from the LMC clusters, NGC 1783 and 1978, are illustrated in Fig. 14, where they fall among the other C stars. van Loon et al. (2003) estimate the period and luminosity for the carbon star,

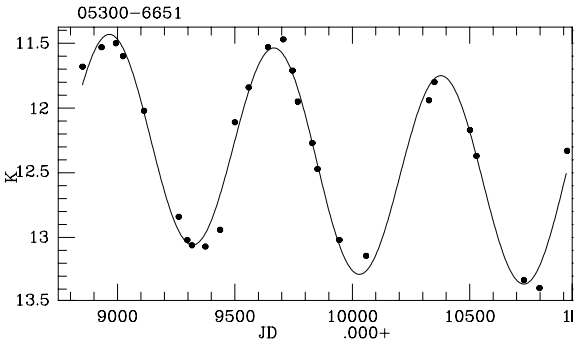

Figure 10. The *K* light curve for IRAS 05300–6651, including data from Wood (1998). The curve is a 708-d sinusoid with a long-term trend (illustrated using a 2832-d sinusoid).

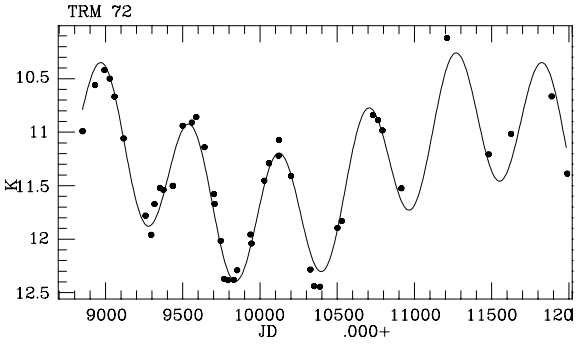

Figure 11. The *K* light curve for TRM 72, including data from Wood (1998). The curve is a 571-d sinusoid with a long-term trend (illustrated using a 2855-d sinusoid).

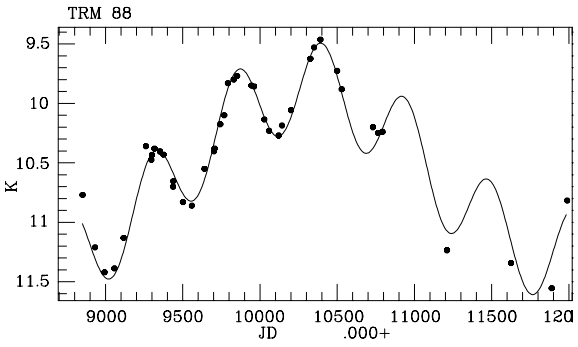

Figure 12. The *K* light curve for TRM 88, including data from Wood (1998). The curve is 544-d sinusoid with a long-term trend (illustrated using a 3266-d sinusoid).

LI-LMC 1813, in the cluster KMHK 1603 as (very approximately) 680 d and $M_{\rm bol} = -5.77$. The turn-off masses for NGC 1783 and 1978 are around 1.5 $M_\odot$ and that of KMHK 1603 is around 2.2 $M_\odot$. Taking this into account, and by analogy with Olivier et al. (2001), we can deduce that the carbon stars in this sample will mostly have had progenitors in the 1.5–2.5 $M_\odot$ range.

Feast et al. (1989) pointed out that stars with periods in excess of 420 d lay above the period–luminosity relation, while Hughes & Wood (1990) specifically derived a PL relation for stars with periods above 400 d – this is illustrated as a dotted line in the various PL diagrams shown here.

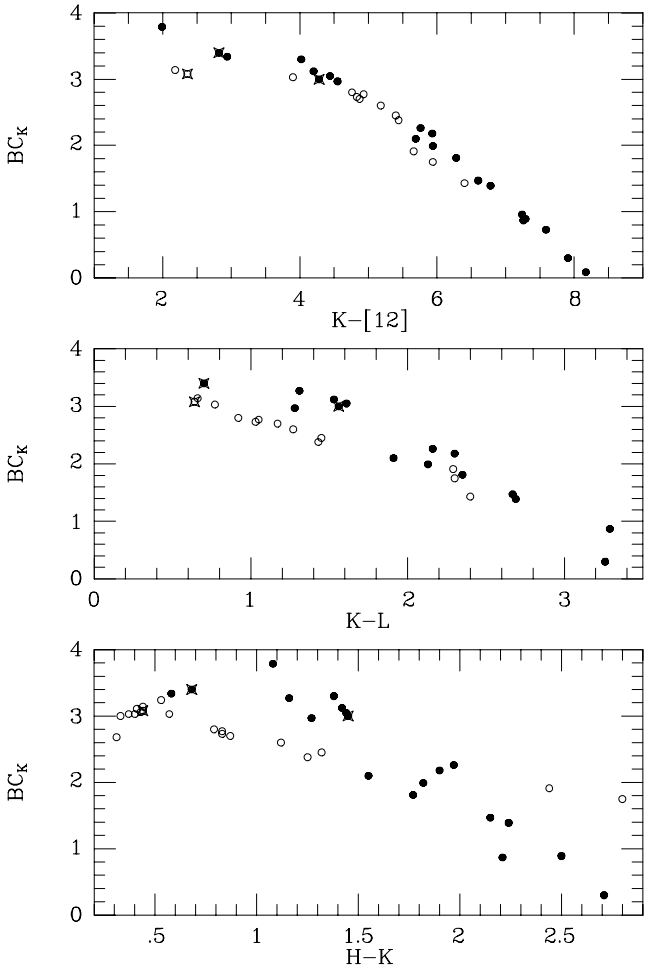

Figure 13. The bolometric correction to *K*, BC_K, as a function of various colours; solid and open symbols are C- and O-rich stars, respectively, while HBB sources are starred.

7.1 Comparison between bolometric magnitudes from *ISO* and *IRAS* data

The differences between the *IRAS* and *ISO* fluxes for these LMC sources were discussed in detail in Paper V, where the *ISO* fluxes were shown to be systematically weaker than those measured by *IRAS*, although systematic selection effects probably contribute to the differences. The fluxes for these sources are close to the observational limit for the *IRAS* experiment, while there is some doubt about the calibration of the *ISO* photometry. Thus it is not clear which measurement should be regarded as more reliable.

A comparison of the long-period ($P > 1000$ d) O-rich sources in the two parts of Fig. 15 shows the bolometric magnitudes from *IRAS* ($\bar{M}_{\rm bol} = -7.03$) to be systematically brighter than those from *ISO* ($\bar{M}_{\rm bol} = -6.76$). In contrast the *IRAS* C-star magnitudes are clearly fainter than those derived from *ISO* data. The difference in the behaviour of the two types of star arises from the application of the colour correction to the *IRAS* data. The measured *IRAS* flux is divided by a factor, f, which is a function of the ratio of the 12–25 μm flux. This correction changes the O-rich fluxes very little because the average value of f is 1.01 and 1.22 for 12 and 25 μm, respectively, while for C stars the mean f is 1.19 and 1.31 for 12 and 25 μm, respectively. It is not possible to derive these corrections with any accuracy given that we have *IRAS* fluxes only at 12 and

Table 4. A comparison of bolometric magnitudes derived from blackbody (BB) and spline (spl) fits.

Name	$m_{\rm bol}$ (BB)	$m_{\rm bol}$ (spl)	BB-spl	$J-K$
O-rich				
SHV 05220–7012	14.71	14.73	−0.02	1.24
SHV 05221–7025	14.35	13.94	0.41	2.78
SHV 05249–6945	13.64	13.63	0.01	1.69
SHV 05305–7022	13.65	13.63	0.02	1.34
R105	13.41	13.44	−0.03	1.37
WBP 74	14.52	14.53	−0.01	1.28
GRV 0517–6551	15.12	14.93	0.19	1.10
RHV 0524–6609	12.74	12.72	0.02	1.30
C-rich				
SHV 05003–6817	13.96	13.55	0.41	3.03
SHV 05003–6829	13.64	13.45	0.19	3.23
SHV 05027–6924	14.09	14.16	−0.07	1.71
SHV 05210–6904	12.84	12.90	−0.06	1.88
SHV 05260–7011	13.90	13.84	0.06	2.98
WBP 14	14.06	14.41	−0.35	2.65
IRAS 05291–6700	13.59	13.44	0.15	2.78

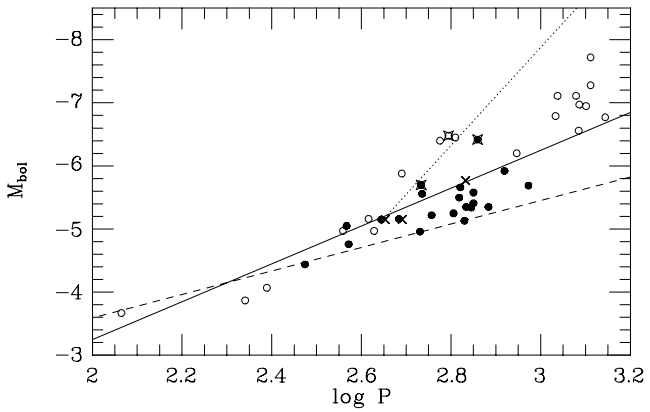

Figure 14. The PL relationship for the LMC sources where the bolometric magnitudes have been calculated from *IRAS* data; solid and open symbols are C- and O-rich stars, respectively, while HBB sources are starred and the crosses represent C stars from LMC clusters (Nishida et al. 2000; van Loon et al. 2003). The solid and dashed lines are extrapolations of the PL relations derived by Feast et al. (1989) for O- and C-rich Miras, respectively, with pulsations periods below 420 d. The dotted line is the relation derived by Hughes & Wood (1990) for AGB stars with periods over 400 d.

25 μm for most of the sources, so this correction procedure is far from ideal.

An interesting feature of the *ISO* observations relates to the four stars for which measurements were obtained on different dates. The bolometric magnitudes derived from these observations are shown in the upper part of Fig. 15 where observations of the same star are connected with vertical bars. These illustrate that bolometric amplitudes of one magnitude are quite possible (see also Papers IV and VI) and suggest that some of the scatter seen in the various PL diagrams must be attributed to variability.

The greater scatter apparent in the upper (*ISO*) diagram in comparison to the lower (*IRAS*) one can be understood in terms of the way the bolometric magnitudes were derived for the two data sets. For the *ISO* diagram they were derived for the specific epoch at which the particular *ISO* observation was obtained, while the *IRAS* diagram makes use of mean magnitudes, both for *JHKL* and from

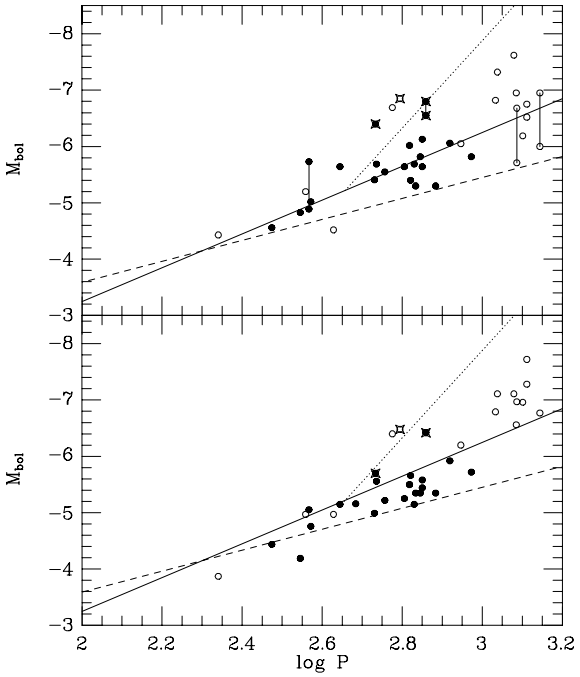

Figure 15. A comparison of the PL relations obtained using *IRAS* (lower) and *ISO* (upper) fluxes, respectively, to calculate the bolometric magnitude, $M_{\rm bol}$. The *IRAS* $M_{\rm bol}$ values are from Table 3 and the *ISO* ones are from Paper VI. The symbols and lines are described in the caption to Fig. 14.

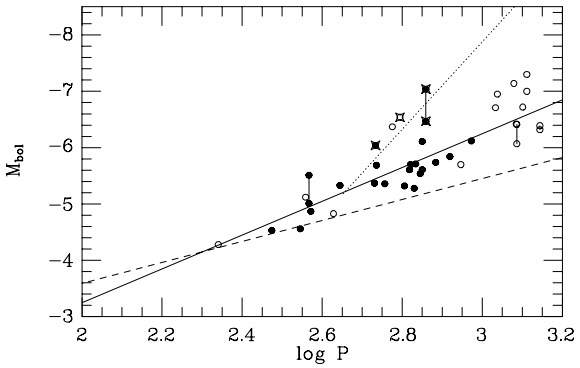

Figure 16. The *ISO* PL relation as shown in Fig. 15 (top), after making a phase correction to approximate the mean magnitude. The symbols and lines are described in the caption to Fig. 14.

IRAS itself (although the *IRAS* mean is obviously not a true value as *IRAS* observed for rather less than a year in total). Fig. 16 illustrates the PL relation derived using the *ISO* data after making a correction to the mean magnitude (the phases are calculated from dates given in Paper V). This correction was estimated by first calculating the bolometric amplitude assuming $\Delta M_{\rm bol} = \log P - 2.0$, then assuming that the bolometric variations are sinusoidal and determining the phase from the K light curve. While the corrections are obviously very uncertain, the procedure does result in a very obvious reduction in the scatter over that seen in Fig. 15 (top).

If the process of deriving means for Fig. 16 was perfect then all of the observations for a particular star would coincide in this diagram, and that is obviously not the case. In particular, the amplitudes of the HBB stars, which are probably low like their K amplitudes (see Section 9) are overestimated as can be seen for IRAS 04496–6958.

It will be seen from the above discussion that it is not possible to make a sensible estimate of the uncertainty associated with the bolometric magnitudes. Variability is clearly significant and values derived from single observations may differ from the mean by up to 0.5 mag, but there are also systematic effects, possibly amounting to as much as a few tenths of a magnitude, which depend on the way colour corrections are treated.

7.2 Comparison with Wood et al. (1992) and Wood (1998)

Wood et al. (1992) obtained near-infrared photometry, measured periods and determined bolometric magnitudes for six of the long-period O-rich stars discussed here, while Wood (1998) did the same for seven of the C stars and one O-rich star (in fact that O-rich star, IRAS 05329–6708, appears in both papers).

The periods reported in these papers are very similar to ours; we determine better values only by combining Wood's data with our own, as discussed in Section 3. However, the luminosities determined by Wood are distinctly different from ours as can be seen from Fig. 17. Both Wood et al. (1992) and Wood (1998) derived bolometric magnitudes, as we do, from a combination of near-infrared and *IRAS* fluxes, although the latter paper also applies an approximate correction to the *IRAS* flux to scale it to the mean light. For the O-rich stars the mean from Wood's data for six stars, $M_{\rm bol} = -6.72 \pm 0.17$, compares with our value of $M_{\rm bol} = -6.91 \pm 0.12$, which is not significant, while for seven C stars the difference is larger with Wood's data giving $M_{\rm bol} = -5.14 \pm 0.17$ compared with our $M_{\rm bol} = -5.45 \pm 0.13$. For IRAS 05329–6708 there is a difference of 0.43 in the bolometric magnitudes quoted by Wood et al. (1992) and the fainter, phase-corrected value quoted by Wood (1998), both points are illustrated in Fig. 17.

Note that three of the C stars illustrated in Fig. 17 (IRAS 05300–6651, TRM 72, TRM 88) are among those with long-term trends discussed in Section 4. Nevertheless, the differences between our magnitudes and those of Wood are not systematically influenced, in any significant way, by our approach to establishing the mean near-infrared magnitudes for these stars. In fact, our bolometric magnitude (−5.56) for TRM 88, which has long-term variations of around $\Delta K \sim 1.0$ mag, is slightly fainter than that derived by Wood (−5.69).

7.3 PL relation: summary

In conclusion we find that, omitting the stars undergoing HBB (see below), both the C- and the O-rich variables tend to follow the trends suggested by an extrapolation of the PL relation determined for shorter-period ($P < 420$ d) stars. There is no clear evidence that these sources with dust shells deviate from the PL relation. They are, however, less luminous than HBB stars with comparable periods. Owing to the uncertainty in the exact mean values of the mid-infrared flux of these stars and therefore in their bolometric magnitudes, it seems inappropriate to attempt to use these data to better define the PL relation.

Wood (1998) particularly emphasizes that the luminosities of the dust enshrouded stars (those with $500 < P < 900$ which we now know are C stars) fall below the extrapolation of the short-period PL relation. This is, however, inconsistent with our findings discussed above.

8 MASS-LOSS RATES

Mass-loss rates were derived in Paper VI (and are listed in Table 3) for many of the stars under discussion and these are used here to examine the mass-loss dependence on the parameters discussed above. For IRAS 04496–6958 we follow Paper VI in adopting the mass-loss rate derived by assuming the dust is pure carbon.

The dependence of mass-loss rate on luminosity was discussed in Paper VI. Given that these stars obey a PL relation we would anticipate a dependence on period, as is indeed seen in Fig. 18. A very similar dependence is seen for Galactic AGB variables (e.g. Whitelock et al. 1994; Olivier et al. 2001). The relation is the same for O- and C-rich stars, just as the PL relation derived from *ISO* data (Fig. 15, top, and Fig. 16) is similar for the two groups. The stars suspected of HBB have lower mass-loss rates than other stars with similar periods. This is of course well known, in that the $P > 420$ d, luminous, O-rich AGB stars, which we now think are undergoing HBB, were discovered visually, while the C stars of comparable period have thick shells and were only discovered via their infrared luminosity.

Given that pulsation is thought to drive mass loss for these stars, some dependence of mass-loss rates on amplitude is to be expected. However, the pulsation amplitude and period are correlated (Fig. 3), making the effects difficult to separate. Fig. 19 shows separate sequences for the O- and C-rich stars, which cross around $\Delta K \sim 1$ mag and $\log \dot{M} \sim -5.5$. At large amplitudes the O-rich stars have both longer periods (higher luminosities) and higher mass-loss rates than do their C-rich counterparts. The HBB stars follow the same trend as the others in this figure.

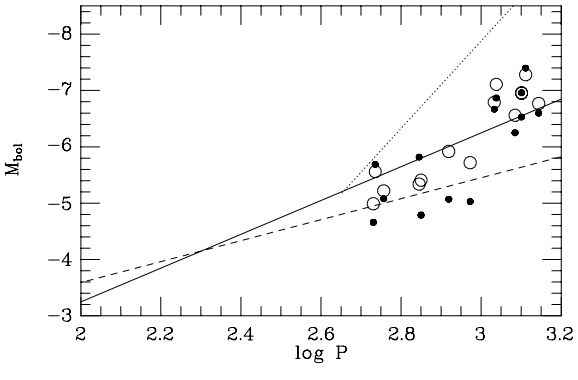

Figure 17. A comparison of the bolometric magnitudes derived here (open circles) and those from Wood et al. (1992) and Wood (1998) (closed circles) for the same sources – note that there are two closed circles for IRAS 05329–6708, one from each paper. The lines are described in the caption to Fig. 14.

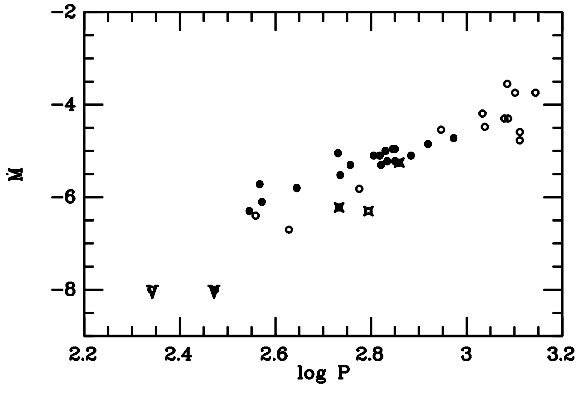

Figure 18. A plot of the mass-loss rate, $\dot{M}$, against the pulsation period, P. Open and closed symbols are O- and C-rich stars, respectively, while stars thought to be undergoing HBB are starred and the upper limits are marked with a V.

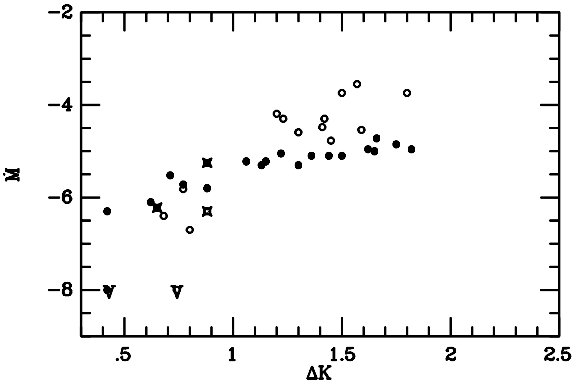

Figure 19. A plot of the mass-loss rate, $\dot{M}$, against the pulsation amplitude, ΔK; symbols as for Fig. 18.

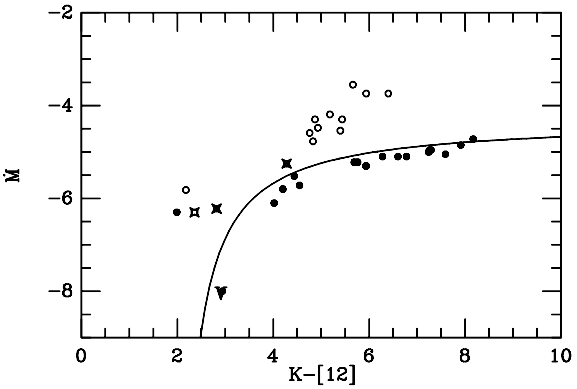

Figure 20. A plot of mass-loss rate, $\dot{M}$, against $K - [12]$ colour; symbols as for Fig. 18. The curve is the relation for galactic C stars derived by Olivier et al. (2001), to provide a qualitative indication of the expectations at low mass-loss rates.

$K - [12]$ is a measure of the optical depth of the dust shell via the relative emission of the star (which dominates the K light) and the shell (which dominates [12]), and is closely dependent on the mass-loss rate (Whitelock et al. 1994). Fig. 20 shows rather different relationships for the O- and C-rich stars in the LMC. Omitting for a moment the clump of four stars at small $K - [12]$, most of the C- and O-rich stars follow qualitatively similar relations to those found for high mass-loss AGB stars in the solar neighbourhood (Olivier et al. 2001), although the O-rich stars in the LMC reach higher mass-loss rates, $\dot{M} > 10^{-4}\,\mathrm{M}_{\odot}\,\mathrm{yr}^{-1}$, at lower $K - [12]$ than do their Galactic counterparts. Galactic stars with $P > 1000$ d have much redder colours as has been discussed elsewhere (e.g. Wood et al. 1992).

The group of four stars with low $K - [12]$ and relatively high $\dot{M}$ comprises two of the three HBB stars, HV 2446, which we would suspect is also undergoing HBB and WBP 14, which has too faint an *IRAS* flux and is probably there erroneously. It is, perhaps, not surprising that the stars undergoing HBB have a different mass-loss versus $K - [12]$ relation from the other AGB stars.

9 HBB STARS

We note that the light-curves for HV 12070, which is known to be HBB, and for HV 2446 and RHV 0524173–660913 (see Fig. 1), which lie in a similar part of the PL diagram (Fig. 15), all have relatively low amplitudes (see Fig. 3). Furthermore, they have similar shapes, exhibiting flat minima (the minima of these particularly bright stars cannot be a consequence of field star contamination).

HV 12070, although O-rich, has an MS spectral type and a rather weak 10-μm silicate feature (Paper V). It is therefore likely that it is very close to the O- and C-rich transition, although it is not possible to say in which direction it is evolving.

The three stars thought to be experiencing, or to have recently experienced, HBB (see Section 1.1) are more luminous than most sources of comparable period. There are many more O-rich S-type stars that fall in the same part of the PL diagram (Feast et al. 1989; Hughes & Wood 1990), i.e. close to the PL relation derived by Hughes & Wood for stars with $P > 400$ d. If the relatively high luminosities for these stars are a consequence of HBB (see also Marigo, Girardi & Bressan 1999) then they may also show high lithium abundances and should be examined spectroscopically. It would also be worth examining the O-rich stars with $P > 1000$ d for lithium.

It is interesting to note that there is a candidate HBB star in IC 1613 that was discovered by Kurtev et al. (2001) and discussed by Whitelock (2003) in the context of AGB stars in Local Group galaxies. It is O-rich, with a spectral type of M3e, has a period of 641 d and is clearly more luminous than an extrapolated PL relation. Its spectrum has not been examined for lithium. Such stars are expected to be a feature of irregular galaxies with significant intermediate-age populations.

10 CONCLUSIONS

Obscured AGB variables with $P > 420$ d have luminosities close to the extrapolation of the PL relation derived for stars with $P < 420$ d. We cannot rule out the possibility that there are fainter obscured AGB stars, which would not have been found to date because of the limited sensitivity of infrared surveys of the LMC.

We suggest that the apparent change in slope of the PL relation around 400–420 d, for stars with thin dust shells, is caused by the inclusion of variables with luminosities brighter than the predictions of the core-mass–luminosity relation, owing to excess flux from HBB.

If RHV 0524173–660913 is confirmed to have changed from an M to a C spectral type (see Section 2) then it is of considerable interest. It is presumably undergoing third dredge-up following a helium-shell flash, possibly because hot bottom burning has just terminated.

ACKNOWLEDGMENTS

We are grateful to Robin Catchpole, John Menzies, Ian Glass and Brian Carter who made some of the *JHKL* observations published here. This paper is based on observations made at the South African Astronomical Observatory.

REFERENCES

Blöcker T., Schönberner D., 1991, A&A, 244, L43
Carter B.S., 1990, MNRAS, 242, 1
Catchpole R.M., Feast M.W., 1981, MNRAS, 197, 385
Feast M.W., Catchpole R.M., Carter B.S., Roberts G., 1980, MNRAS, 193, 377
Feast M.W., Glass I.S., Whitelock P.A., Catchpole R.M., 1989, MNRAS, 241, 375
Feast M., Whitelock P., Menzies J., 2002, MNRAS, 329, L7
Ferraro F.R., Fusi Pecci F., Testa V., Greggio L., Corsi C.E., Buonanno R., Terndrup D.M., Zinnecker H., 1995, MNRAS, 272, 391

Frost C.A., Cannon R.C., Lattanzio J.C., Wood P.R., Forestini M., 1998, Astron. Lett., 332, 17
Gaposchkin S., 1970, Smithsonian Astrophys. Obs. Spec. Rep., no 310,
Glass I.S., Whitelock P.A. Catchpole R.M., Feast M.W., Laney C.D., 1990, SAAO Circ., 14, 63
Groenewegen M.A.T., Whitelock P.A., 1996, MNRAS, 281, 1347
Hughes S.M.G., Wood P.R., 1990, AJ, 99, 784
Kurtev R., Georgiev L., Borissova J., Li W.D., Filippenko A.V., Treffers R.R., 2001, A&A, 378, 449
Loup C., Zijlstra A.A., Waters L.B.F.M., Groenewegen M.A.T., 1997, A&AS, 125, 419 (Paper I)
Marigo P., Girardi L., Bressan A., 1999, A&A, 344, 123
Mouhcine M., Lançon A., 2002, A&A, 393, 149
Nishida S., Tanabé T., Nakada Y., Matsumoto S., Sekiguchi K., Glass I.S., 2000, MNRAS, 313, 136
Olivier E.A., Whitelock P., Marang F., 2001, MNRAS, 326, 490
Payne-Gaposchkin C.H., 1971, Smithsonian Contrib. Astrophys., no 13
Reid N., Glass I.S., Catchpole R.M., 1988, MNRAS, 232, 53
Reid N., Hughes S.M.G., Glass I.S., 1995, MNRAS, 275, 331
Sackmann I.-J., Boothroyd A., 1992, ApJ, 392, L71
Smith V.V., Plez B., Lambert D.L., Lubowich D.A., 1995, ApJ, 441, 735
Trams N.R. et al., 1999a, A&A, 344, L17
Trams N.R. et al., 1999b, A&A, 346, 843 (Paper V)
van Loon J. Th., Zijlstra A.A., Whitelock P.A., Waters L.B.F.M., Loup C., Trams N.R., 1997, A&A, 325, 585 (Paper III)
van Loon J. Th. et al., 1998, A&A, 329, 169 (Paper IV)
van Loon J. Th., Groenewegen M.A.T., de Koter A., Trams N.R., Waters L.B.F.M., Zijlstra A.A., Whitelock P.A., Loup C., 1999, A&A, 351, 559 (Paper VI)
van Loon J. Th., Marshall J.R., Matsuura M., Zijlstra A.A., 2003, MNRAS, in press (astro-ph/0302083)
Westerlund B.E., Olander N., Hedin B., 1981, A&AS, 43, 267
Whitelock P., 2003, in Nakada Y., Honma M., eds, Mass-Losing Pulsating Stars and Their Circumstellar Matter. Kluwer, Dordrecht, ASSL, in press
Whitelock P.A., Feast M.W., 2000, Mem. Soc. Astron. Ital., 71, 601
Whitelock P., Menzies P., Feast M., Marang F., Carter B., Roberts G., Catchpole R., Chapman J., 1994, MNRAS, 267, 711
Whitelock P.A., Feast M.W., Marang F., Overbeek M.D., 1997, MNRAS, 288, 512
Winters J.M., Fleischer A.J., Gauger A., Sedlmayr E., 1994, A&A, 290, 623
Wood P.R., 1998, A&A, 338, 592
Wood P.R., Bessell M.S., Paltoglou G., 1985, ApJ, 290, 477
Wood P.R., Whiteoak J.B., Hughes S.M.G., Bessell M.S. Gardner F.F., Hyland A.R., 1992, ApJ, 397, 552
Zijlstra A.A., Loup C., Waters L.B.F.M., Whitelock P.A., van Loon J. Th., Guglielmo F., 1996, MNRAS, 279, 32 (Paper II)

This paper has been typeset from a TEX/LATEX file prepared by the author.